HHS Public Access

Author manuscript

Cell Rep. Author manuscript; available in PMC 2021 October 28.

Published in final edited form as:

Cell Rep. 2021 July 06; 36(1): 109333. doi:10.1016/j.celrep.2021.109333.

Altered conformation of α-synuclein drives dysfunction of synaptic vesicles in a synaptosomal model of Parkinson's disease

Luis Fonseca-Ornelas[1], **Thibault Viennet**[2,3], **Matteo Rovere**[1], **Haiyang Jiang**[1], **Lei Liu**[1], **Silke Nuber**[1], **Maria Ericsson**[4], **Haribabu Arthanari**[2,3], **Dennis J. Selkoe**[1,5,*]

[1]Ann Romney Center for Neurologic Diseases, Brigham and Women's Hospital and Harvard Medical School, Boston, MA 02115, USA

[2]Cancer Biology, Dana-Farber Cancer Institute, Boston, MA 02115, USA

[3]Biological Chemistry and Molecular Pharmacology, Harvard Medical School, Boston, MA 02115, USA

[4]Electron Microscopy Laboratory, Department of Cell Biology, Harvard Medical School, Boston, MA 02115, USA

[5]Lead contact

SUMMARY

While misfolding of alpha-synuclein (αSyn) is central to the pathogenesis of Parkinson's disease (PD), fundamental questions about its structure and function at the synapse remain unanswered. We examine synaptosomes from non-transgenic and transgenic mice expressing wild-type human αSyn, the E46K fPD-causing mutation, or an amplified form of E46K ("3K"). Synaptosomes from mice expressing the 3K mutant show reduced Ca^{2+}-dependent vesicle exocytosis, altered synaptic vesicle ultrastructure, decreased SNARE complexes, and abnormal levels of certain synaptic proteins. With our intra-synaptosomal nuclear magnetic resonance (NMR) method, we reveal that WT αSyn participates in heterogeneous interactions with synaptic components dependent on endogenous αSyn and synaptosomal integrity. The 3K mutation markedly alters these interactions. The synaptic microenvironment is necessary for αSyn to reach its native conformations and establish a physiological interaction network. Its inability to populate diverse conformational ensembles likely represents an early step in αSyn dysfunction that contributes to the synaptotoxicity observed in synucleinopathies.

In brief

*Correspondence: dselkoe@bwh.harvard.edu.

AUTHOR CONTRIBUTIONS

L.F.-O. and D.J.S. designed the research. L.F.-O., T.V., M.R., H.J., L.L., S.N., and M.E. performed the research. L.F.-O., T.V., H.A., and D.J.S. analyzed the data. L.F.-O., T.V., and D.J.S. initially wrote the manuscript, and all authors contributed to editing it.

DECLARATION OF INTERESTS

D.J.S. is a director of and consultant to Prothena Biosciences. All other authors declare no competing interests.

SUPPLEMENTAL INFORMATION

Supplemental information can be found online at https://doi.org/10.1016/j.celrep.2021.109333.

Fonseca-Ornelas et al. report the in-cell NMR behavior of αSyn at synapses. While WT αSyn participates in transient interactions with synaptic components, an αSyn variant based on an fPD mutant displays a reduced ability to do so. This results in biochemical, morphological, and functional changes that may explain αSyn-related toxicity.

Graphical Abstract

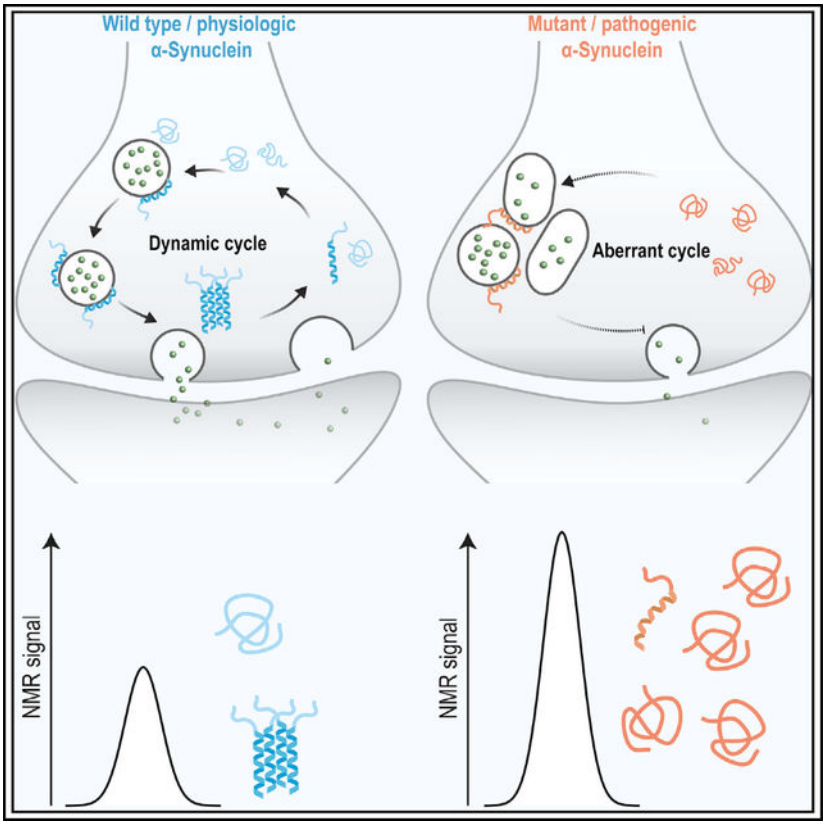

INTRODUCTION

Parkinson's disease (PD), dementia with Lewy bodies (DLB), and other synucleinopathies are characterized by the misfolding of α-synuclein (αSyn), a neuronal protein enriched at presynaptic terminals (George et al., 1995). Misfolded αSyn can form Lewy bodies, the diagnostic hallmarks of these disorders (Shahmoradian et al., 2019; Spillantini et al., 1997). Missense mutations, duplications, or triplications of the *SNCA* gene each cause familial forms of PD (Fujishiro et al., 2013; Nussbaum, 2016). αSyn's membrane-binding N terminus harbors seven imperfect repeats with a KTKEGV consensus sequence, which modulate its transient interaction with curved membranes and its folding into an α-helical secondary structure (Davidson et al., 1998; Fusco et al., 2014; Jo et al., 2000). αSyn also has a hydrophobic "non-amyloid-β component" (NAC) region implicated in its self-aggregation (Fonseca-Ornelas et al., 2014; Giasson et al., 2001) and a negatively charged C-terminal domain. Although αSyn function is still debated (Lautenschläger et al., 2018; Man et al., 2021; Runwal and Edwards, 2021), compelling evidence suggests that it acts as a chaperone

that contributes to the assembly of SNARE (soluble N-ethylmaleimide-sensitive fusion protein [NSF] attachment protein receptor) complexes through both protein-protein and protein-lipid/membrane interactions at the presynaptic terminal (Burré et al., 2012). It has been hypothesized that this process enables αSyn to help regulate the trafficking of synaptic vesicles (SVs) and thereby neurotransmitter release (Atias et al., 2019; Burré et al., 2010; Logan et al., 2017; Nemani et al., 2010; Winner et al., 2011).

Evidence from our and other groups suggests that physiological αSyn occurs in an equilibrium between an unfolded, monomeric species (M) and a helically folded, tetrameric (T) conformation that may be both cytosolic and membrane-bound (Bartels et al., 2011; Burré et al., 2014; Dettmer et al., 2013, 2016). Missense mutations that cause familial PD all decrease the cellular T:M ratio and promote the accumulation of αSyn in its monomeric form (Dettmer et al., 2013, 2015a; Westphal and Chandra, 2013). Decreased T:M ratios of endogenous human αSyn have also been observed in induced pluripotent stem cell (iPSC)-derived neurons from patients with PD carrying loss-of-function mutations in glucocerebrosidase A (GBA) (Kim et al., 2018). Molecular modeling also suggests that a folded tetramer is the αSyn structure with the lowest apparent activation energy (Cote et al., 2018; Xu et al., 2019).

Recent work by our group has also shown that “amplifying” the familial PD (fPD)- and DLB-causing E46K (“1K”) mutation by inserting analogous E→K substitutions into one or both of the two adjacent KTKEGV repeats (+E31K yielding “2K,” and +E61K yielding “3K”) can further decrease tetramers, sequester αSyn in its monomeric state, and increase its affinity for membranes, causing neuronal dysfunction and pathology. Expressing the 3K αSyn mutant in mouse primary neurons and human iPSC-derived neurons induces cytotoxicity and the formation of round cytoplasmic vesicle-rich inclusions containing clusters of vesicles and tubules (Dettmer et al., 2017). Transgenic mice expressing the tetramer-reducing 3K mutation develop a striking PD-like motor phenotype (including resting tremor and limb and gait deficits) that advances with age and responds to acute L-DOPA administration (Nuber et al., 2018). In the brains of these 3K mice, round cytoplasmic deposits occur and the excess monomers are more prone to bind to membranes and become more abundant than tetramers (Dettmer et al., 2015b; Nuber et al., 2018). A mouse line with homozygous expression of the 3K mutation at low levels similar to those of endogenous αSyn (referred to as $3KL^{+/+}$ mice) presents the same, yet delayed and milder PD-like motor deficits (Nuber et al., 2018). Based on these emerging findings, we hypothesize that the physiological state of αSyn includes metastable multimers in equilibrium with unfolded monomers and any dyshomeostasis can result in neuronal pathology. However, the effects of fPD and fPD-like mutations on the conformational dynamics of αSyn at intact presynaptic environments remain unexplored. To address this, we analyzed αSyn in synaptosomes—nerve terminals that are “pinched off” during brain homogenization and immediately resealed (Whittaker, 1993). Synaptosomes can be purified and retain many characteristics of intact synaptic boutons: They have abundant SVs and exhibit dense molecular crowding, respiratory activity, membrane potentials, Ca^{2+}-dependent neurotransmitter release, and responsivity to neuropharmacological agents (Evans, 2015; Nishida et al., 2004; Whittaker, 1993; Wiedemann et al., 1998). Because αSyn displays affinity for the surface of small vesicles with highly curved membranes

(Clayton and George, 1998; Perrin et al., 2001; Rovere et al., 2019), influences synapse structure (Vargas et al., 2017), and regulates the size (Medeiros et al., 2017), distribution, and recycling of SVs (Atias et al., 2019; Fortin et al., 2004, 2005; Sun et al., 2019), we posit that an impaired ability of PD-causing αSyn mutants to exchange between conformations and interact with its synaptosomal partners might dysregulate synapse homeostasis and leave excess monomers available to initiate synaptotoxic processes (Dettmer et al., 2015b; Nuber et al., 2018). By combining biochemical and functional assays, transmission electron microscopy, and an intra-synaptosomal approach of nuclear magnetic resonance (NMR) spectroscopy, we examined the changes that αSyn induces in synaptosomes isolated from our homozygous $3KL^{+/+}$ mice displaying a PD-like phenotype. We found that the $3KL^{+/+}$ brain synaptosomes have impaired SNARE-complex assembly, atypical SV morphology, and reduced Ca^{2+}-dependent SV exocytosis compared to those of non-transgenic (NTG) and wild-type (WT) human (hu) αSyn mice. Furthermore, the 3K synaptosomes have abnormal levels and distribution of select proteins relevant to synaptic vesicle trafficking and neurotransmitter release. We then introduced recombinant ^{15}N-labeled WT or 3K hu αSyn into intact synaptosomes and used NMR to analyze αSyn molecular behavior inside the crowded milieu of the sealed synaptosome. This ion-, protein-, and lipid-rich environment promoted NMR changes in WT hu αSyn that had not been observed in previous structural analyses of the recombinant protein in solution nor in previous in-cell NMR studies (Theillet et al., 2016), suggesting that αSyn can dynamically populate different conformational ensembles in different microenvironments. By contrast, the ^{15}N-labeled 3K mutant appeared to adopt an ensemble of conformations more closely resembling that of unfolded, monomeric αSyn in solution *in vitro*. In synaptosomes from mice lacking endogenous αSyn (SNCA KO), electroporated WT αSyn no longer showed the dynamic NMR changes of the N-terminal region observed within synaptosomes from mice with endogenous αSyn (NTG mice), suggesting that the NMR behavior we observe in synaptosomes requires interaction between the introduced unfolded αSyn and endogenous αSyn. The synapse is an environment in which αSyn populates an array of dynamic conformations. Still, pathogenic mutations decrease its interaction capabilities with the synaptosomal milieu and induce alterations in the biochemistry, activity, and ultrastructure of synaptic vesicles.

RESULTS

Altered ultrastructure and reduced SV docking in brain synaptosomes from the $3KL^{+/+}$ mouse model of PD is associated with decreased Ca^{2+}-dependent exocytosis

It has been reported that abnormal αSyn presence at the synapse has detrimental effects on synaptic architecture and vesicle recycling activity (Fortin et al., 2005; Logan et al., 2017; Medeiros et al., 2017). Following our previous findings showing that the 3K mutation leads to an increase in aggregation-prone αSyn monomers (Dettmer et al., 2015b; Nuber et al., 2018), we examined the ultrastructural effects of αSyn and its fPD-related mutants on mouse synaptosomes (Figure 1A). Synaptosomes isolated from the brains of NTG or transgenic hu WT αSyn, E46K, and $3KL^{+/+}$ (a transgenic line expressing low levels of the amplified 3K αSyn mutant) had similar SV number and distribution as well as abundance of mitochondria and active zone length (Figure S1A). However, size quantification of SVs

from 3KL$^{+/+}$ mice revealed larger mean diameters than the SVs in E46K, hu WT αSyn, and NTG synaptosomes (Figures 1B–1E, quantification in Figure 1K). Moreover, elongated SVs, also described as cisternae (Medeiros et al., 2017), were significantly more abundant in the 3KL$^{+/+}$ synaptosomes, representing ~12% of total SVs in these fractions, significantly above the ~6.8% and 7.0%, and 9.7% of elongated SVs present in NTG, hu αSyn WT, and E46K mice synaptosomes, respectively (Figures 1B–1E, white arrowheads; quantification in Figure 1J).

αSyn overexpression has been reported to have detrimental effects on the availability of SVs for docking to the plasma membrane and the overall integrity of postsynaptic densities (Kohl et al., 2016; Nemani et al., 2010). Ultrastructural analysis of our 3KL$^{+/+}$, E46K, hu WT αSyn, and NTG synaptosomes revealed no significant difference in the total number of SVs and the average length of the active zones among the four genotypes (Figure S1A). However, the number of SVs docked at the active zone (SVs within ~30 nm of the plasma membrane) was significantly reduced in the 3KL$^{+/+}$ synaptosomes (Figures 1F–1I, arrows; quantified in Figure 1L). Synaptosomes from mice harboring the E46K mutation showed percentages of altered SVs shape and numbers of SVs docked at the active zone that fell in between the WT and 3KL$^{+/+}$ synaptosomes, supporting *in vitro* and *in vivo* evidence that the effects of the 3K mutation represent an additive influence on the phenotypes of the fPD-causing E46K (Dettmer et al., 2015a; Nuber et al., 2018).

We then inquired whether the altered shape of SVs and their reduced docking to the active zone in the 3KL$^{+/+}$ synaptosomes had a measurable effect on their functional activity. We used the lipophilic styryl dye FM2–10, which increases its fluorescence when incorporated into the luminal leaflet of the SV membrane during endocytosis. Accumulated FM2–10 is discharged during exocytosis, promoting a decrease in its fluorescence (Baldwin et al., 2003; Rizzoli and Betz, 2004). We determined that the Ca^{2+}-dependent fluorescence decay observed in NTG, hu αSyn WT, and, to a lesser extent, E46K synaptosomes was significantly faster than in 3KL$^{+/+}$ synaptosomes (Figure 1M). Ca^{2+} influx is the trigger of synaptic vesicle exocytosis, and faster decay kinetics correspond to faster vesicle recycling and release. We conclude that 3KL$^{+/+}$ synaptosomes exhibit impaired exocytic activity, in addition to the abnormal SV morphology and reduced docking on synaptic plasma membranes we observed by ultrastructural analysis. Since αSyn aggregation is a critical mechanism of pathogenesis of PD, we assessed the fibrilization propensity of the E46K and 3K variants of αSyn and compared them with that of the WT protein. We quantified the formation of amyloid fibrils with Thioflavin-T (ThT) fluorescence (Figure S1B). In agreement with a previous study (Flagmeier et al., 2016), the E46K and 3K mutations had little effect on aggregation kinetics when compared to WT αSyn (Figure S1B). We conclude that the consistent changes in synaptosomal ultrastructure and activity from the 3KL$^{+/+}$ brains are not likely to be due to enhanced αSyn aggregation.

Synaptosomes from the αSyn 3KL$^{+/+}$ PD mouse model have altered levels of select synaptic proteins and reduced SNARE complex assembly

A widely hypothesized function of αSyn is to participate in synaptic vesicle fusion and recycling, either by itself (Fusco et al., 2016) or by acting as a chaperone for SNARE

complexes (Burré et al., 2010, 2012). We therefore analyzed the distribution and relative abundance of numerous synaptic proteins in total brain homogenates and their cytosolic and synaptosomal fractions (Figure S2). Proteins involved in the synaptic vesicle loading system (Rab-3A, synaptophysin, synaptobrevin), in the docking and priming of vesicles in the active zone (CASK, syntaxin-1, complexin), in the regulation of endocytotic events and vesicle uncoating (amphiphysin, HSC70), and in the postsynaptic density (PSD95) showed decreased levels in the synaptosomes of $3KL^{+/+}$ mice (Figures 2A and 2B). In some cases, we observed a dose-dependent effect on the levels of these synaptic components, wherein the overexpression of both hu WT and E46K αSyn lowered their abundance compared to the NTG synaptosomes. The decrease, however, was more prominent in the synaptosomes of $3KL^{+/+}$ mice. Since the total amounts of the synaptic proteins mentioned above were unchanged in the homogenates of brains from the four genotypes (Figure S2: homogenate fraction), the differences we find in the synaptosomes likely represent altered protein localization to synapses, rather than overall expression levels.

The amount of αSyn differs among the four genotypes, as $3KL^{+/+}$ transgenic mice express more αSyn than NTG but less than transgenic hu WT αSyn and E46K animals (Figures 2A and 2B: αSyn blot). However, these differences in αSyn abundance do not correlate with the effects observed at the ultrastructural, biochemical, and functional levels among the four genotypes, demonstrating that the changes mentioned above result from the introduction of the 3K mutation and not from the overall levels of αSyn expression.

Given the reported role of αSyn in chaperoning the assembly of SNARE complexes (Burré et al., 2010), we asked whether the presence of the 3K mutant affected this assembly process. We quantified the SNARE-complex assembly by immunoblotting of non-boiled samples for SNAP25, synaptobrevin, and syntaxin. We found that the synaptosomal fractions from E46K and $3KL^{+/+}$ brains have reduced SNARE-complex assembly compared to those from the hu WT αSyn and NTG mice (Figure 2C).

Inside synaptosomes, αSyn populates conformational ensembles different than soluble, unfolded monomers

Given the multiple biochemical and ultrastructural changes in mutant αSyn-expressing synaptosomes described above, we proceeded to characterize by NMR the molecular behavior of WT and 3K αSyn at residue-specific resolution inside the physiologically relevant environment of a synaptosome. When we simply spiked NMR-visible ^{15}N-labeled recombinant αSyn into a purified synaptosome sample (Figure S3A), it remained outside of the intact synaptosomes, and its NMR spectrum showed no discernible differences from that of αSyn in saline buffer (NMR buffer; see STAR Methods). This lack of NMR signal change indicates that no dynamic processes—such as interactions with the outer leaflet of synaptosomal membranes—had occurred (Figures S3B and S3C). Because we were interested in the behavior of αSyn inside synaptosomes, we designed a modified version of in-cell NMR (Theillet et al., 2016) in which protein electroporation (Ramanathan et al., 2000) is used to deliver either ^{15}N or ^{13}C isotope-enriched human αSyn into purified synaptosomes. To establish whether the observed NMR signals came from the αSyn inside the synaptosomes, immediately after the electroporation pulses, we performed a

trypsin treatment to remove non-internalized, extra-synaptosomal protein (Alex et al., 2019), followed by a sodium carbonate (pH 11) wash to remove membrane-associated proteins, and a final wash with NMR buffer (see STAR Methods). After these steps, the electroporated exogenous αSyn remained inside the intact synaptosomes and was shielded from trypsin cleavage (Figure 3A). We also found no significant leakage or degradation of either the recombinant αSyn or endogenous SNAP25 and glutaminase from the synaptosomes over the first 4 h post-electroporation (Figure 3B). Accordingly, we restricted the length of all of our NMR measurements to 4 h, during which the loss in protein signal represented <15% of the initial value of added recombinant αSyn (Figure 3B). Similarly, we used immunofluorescent confocal microscopy and immunogold transmission electron microscopy to confirm that, after the washes, the exogenously delivered WT human αSyn appeared uniformly distributed within synaptosomes, adopting a similar localization to that of the endogenous murine αSyn (Figures 3C and 3D). We performed semiquantitative western blotting to evaluate the concentration of recombinant αSyn inside the synaptosomes, by using a dilution series of known amounts of recombinant αSyn compared with the electroporated synaptosomal samples. We estimated an intra-synaptosomal αSyn concentration after the electroporation and washing steps for both the WT and 3K human αSyn of 8–14 μM (Figure 4A; Figure S4C), thus excluding differences in electroporation efficiency of the two αSyn variants and in line with the values observed in previous in-cell αSyn NMR studies (Binolfi et al., 2016; Burmann et al., 2020; Theillet et al., 2016) and with the estimates of intracellular αSyn physiological concentration (Wilhelm et al., 2014).

To compare intra-synaptosomal concentrations of electroporated αSyn obtained by western blot (WB) with the observed NMR signals, we performed a one-dimensional (1D) ^{15}N-filtered NMR experiment on intra-synaptosome αSyn and compared it to the same concentration of αSyn in NMR buffer at pH 6.6, similar to the pH inside synaptosomes (Deutsch et al., 1981; Nachshen and Drapeau, 1988). NMR signals from αSyn inside the synaptosomes were lower than what was expected for a ~14 μM sample (Figure 4B). This decrease was significantly more pronounced for the WT hu αSyn, which generated only about 28% of the expected NMR signal, compared to ~48% of the expected signal for the 3K variant (Figure 4B). We then compared two-dimensional ^{1}H-^{15}N heteronuclear single-quantum coherence (HSQC) experiments of exogenous WT and 3K αSyn inside synaptosomes with reference spectra of each αSyn in NMR buffer at pH 6.6. The C-terminal regions of both WT and 3K αSyn within synaptosomes showed significant combined chemical shift perturbations (CSPs), well above 0.1 ppm, (Figure 4C, quantified in Figure 4E) accompanied by a ~60%–80% line broadening (i.e., signal attenuation) particularly notable in residues Y125 and Y133 (Figure 4C, quantified in Figure 4E). The spectral changes of the N-terminal residues of intra-synaptosomal WT and 3K αSyn were more striking. Their ^{1}H-^{15}N signals showed significant signal attenuation compared to those of the unfolded, monomeric αSyn in buffer but few CSPs (Figure 4D, blue and orange profiles, respectively). Interestingly, while the first ~60 residues of both 3K and WT hu αSyn lost comparable signal intensity inside the synaptosomes, the region encompassing residues 61 to 110 (NAC domain) of the 3K variant was significantly less affected by the intra-synaptosomal environment than that of WT, as evidenced by an overall signal loss of only 32%, compared to the more than 60% loss for the WT protein (Figure

4E). Importantly, DSG cross-linking trapped the intra-synaptosomal recombinant αSyn in multimeric conformations similar to those we have described in intact living cells (Dettmer et al., 2013, 2015a, 2015b) (Figure 5F). While both WT and 3K αSyn had DSG-trapped multimeric assemblies inside synaptosomes, the monomeric form of 3K was significantly more abundant, showing a 50% reduction of its multimer:monomer ratio compared to the WT protein (Figures 5F and 5H). The higher monomeric accumulation detected by western blot of the 3K variant thus correlates with its higher NMR signal intensity.

The multimerization of exogenous αSyn depends on synapse integrity and the presence of endogenous αSyn

The NMR signal attenuation shown in Figure 4D could result from any one or a combination of the following factors: (1) intermediate exchange contribution due to amide proton exchange with water (dependent on pH and ionic strength); (2) slower molecular tumbling due to higher viscosity; (3) intermediate exchange contributions due to transient interactions with low-molecular-weight partners (ions, small molecules, small proteins); (4) slower molecular tumbling due to tight interaction with high-molecular-weight partners (membranes, vesicles, large proteins, oligomers); (5) intermediate exchange contribution from different conformations of monomeric αSyn or multimerization events with the (NMR-invisible) endogenous mouse αSyn. To deconvolute each one of these five possibilities, we performed the following control experiments.

pH—NMR intensities in two-dimensional ^{1}H-^{15}N HSQC experiments are sensitive to hydrogen exchange. Because of the reported pH (~6.6) inside synaptosomes (Deutsch et al., 1982; Nachshen and Drapeau, 1988), we performed a pH titration of both WT and 3K αSyn in buffer to exclude pH changes and hydrogen exchange effects as explanations for our findings involving changes in amide signal intensity (Figure S3D). As expected, intensities along the N-terminal region of αSyn increased with lowering pH from 7.4 to 7.0, and 6.6 (Figure S3E). Using the chemical shift of histidine 50 (Figure S3D, black arrow; quantified in Figures S3G and S3H) as a proxy for pH, we were able to approximate the pH inside synaptosomes as closer to 6.6 than to the 7.4 we used in buffers throughout the synaptosome purification and electroporation protocols. This suggested that the synaptosomes were reasonably intact and their proton pumps active during the close to 7 h our protocol takes from mouse brain extraction to NMR measurement. Additionally, because carbon-bound hydrogen atoms are much less prone to exchange with water (and thus are less affected by pH), we also measured the broadening of methyl proton peaks via selective optimized flip angle short transient (SOFAST) heteronuclear multiple quantum coherence (HMQC) (Figure S4). Here, the signals of αSyn are also attenuated upon introduction into the synaptosomes: The WT αSyn loses around 83% of its expected signal in buffer (Figure S4D), while the 3K αSyn signal is only broadened to about 38% of its expected signal in buffer. Taken together, these experiments show that our observations of αSyn NMR signal attenuation inside synaptosomes are not driven by hydrogen exchange.

Crowding—In the presence of the biologically inert crowding agents Percoll and iodixanol, αSyn NMR signal *in vitro* did not show any discernible attenuation nor CSP (Figure S5), suggesting that the line broadening we observed before when αSyn was electroporated

inside synaptosomes is not a result of increased medium viscosity and molecular crowding alone (Minton, 2001; Selenko et al., 2008).

Calcium ions and intact local concentration—The C-terminal effects described above closely resemble reported NMR data on αSyn *in vitro* in the presence of a high concentration of Ca^{2+}, which may play a role in the localization of αSyn at the presynaptic terminal in response to neuronal activity (Lautenschläger et al., 2018). We hypothesized that the same effect could be taking place inside the Ca^{2+}-rich environment of synaptosomes, so we performed our whole synaptosomal NMR sample preparation in the presence of the Ca^{2+} ion chelator EGTA. Indeed, EGTA (1 mM) abolished the significant CSP observed in the C-terminal region, but not the changes in intensity in the N-terminal and NAC regions (Figure S6). These results suggests that the final ~45 residues of αSyn interact with Ca^{2+} through the multiple negatively charged residues that populate this domain. While EGTA abolished the CSP at the C-terminal region, it only slightly decreased the line-broadening effect, so additional processes such as molecular crowding and protein-protein interactions are presumably occurring in this region, likely with molecular chaperones as interactans (Burmann et al., 2020; Burré et al., 2012; Lautenschläger et al., 2018). We also noted that EGTA reversed the line-broadening of the first 15 residues almost completely, as expected due to electrostatic “shielding” of the interaction between αSyn and negatively charged lipid head groups (Bertoncini et al., 2005). Finally, we subjected the synaptosomes electroporated with ^{15}N-labeled αSyn to vigorous sonication to lyse them. In subsequent HSQC experiments, both WT and 3K αSyn showed little or no backbone amide CSP in the NAC and C-terminal regions (Figures S6G and S6H). This may be because a high local concentration of Ca^{2+} is necessary to induce the C-terminal effects, and this local concentration becomes markedly diluted upon synaptosomal lysis. Moreover, line-broadening was restricted to the first ~35 residues of the N-terminal region of both WT and 3K αSyn, in line with the reported transient lipid interactions of αSyn with vesicles that are highly abundant in synaptosomes (Rovere et al., 2018a; Viennet et al., 2018). Additional signal broadening in the final ~25 residues of the C-terminal region was also maintained and is reminiscent of previously described NMR profile of αSyn inside cells (Burmann et al., 2020) (Figure S6I). In the 3K mutant, we further found line broadening in the residues surrounding the 3 E→K substitutions at positions 35, 46, and 61 compared to a sample of 3K αSyn in buffer (Figure S6I, red lines), suggesting that higher affinity for membranes or macromolecular interactions exclusive to the 3K protein are taking place (Rovere et al., 2019), in line with 3K αSyn being enriched in brain membrane fractions of transgenic mice (Nuber et al., 2018). These findings imply that the dynamic NMR behavior of αSyn requires the intact milieu of the synaptosome, as diluted synaptic components (i.e., in lysates post-sonication) are not sufficient to fully recapitulate these effects.

The role of endogenous αSyn—Using synaptosomes purified from αSyn-KO mice (Figure 5), we found that in the absence of endogenous αSyn, the NMR signal attenuation in the N-terminal region of exogenously delivered αSyn was far less prominent for both WT and 3K αSyn (Figure 5E). We also found that DSG cross-linking trapped significantly fewer multimers in αSyn-KO synaptosomes than in those of NTG mice harboring endogenous murine αSyn (Figures 5G and 5H). Other than the lack of endogenous αSyn, the αSyn-

KO synaptosomes have the same components as NTG synaptosomes, suggesting that the endogenous αSyn has an essential role in the molecular mechanisms that promote the signal attenuation of the exogenously introduced recombinant αSyn. These KO data also show that the NMR effects we observed are not primarily due to slower molecular tumbling resulting from interaction with synaptic membranes or other large molecular weight partners.

DISCUSSION

The results reported here suggest that the molecular behavior of αSyn inside intact synaptosomes influences both the morphology and function of synaptic vesicles and that its dyshomeostasis can result in the cellular toxicity and PD-like motor phenotypes observed in $3KL^{+/+}$ mice.

Synaptosomes isolated from the brains of $3KL^{+/+}$ mice carrying the E→K mutations that destabilize αSyn's multimerization have altered morphology and size of SVs (Figures 1J and 1K), a reduced number of SVs docked to the active zone (Figure 1L), and decreased SNARE-complex assembly (Figure 2B). All of these changes likely contribute to the demonstrated impairment of SV membrane fusion and recycling activity (Figure 1M). These alterations of synaptosomes from the 3K brain are associated with decreased levels of proteins involved in all facets of synapse function and architecture, from SV loading to docking, priming, and fusion at the active zone, as well as endocytosis and the postsynaptic density (Figure 2A). While overexpression of WT or E46K αSyn has detrimental effects on the ultrastructure, biochemistry, and activity at the synapse, it is the 3K mutation that consistently shows a more marked phenotype despite expressing far less αSyn than the hu WT and E46K transgenic mice (Figure 2A, αSyn blot). Collectively, the combination of biochemical, ultrastructural, and functional data in these four mouse lines indicates that the presence of a rationally designed, amplified form of the fPD-causing E46K mutant impairs synaptic homeostasis independently from total αSyn levels and that the abnormal accumulation of some SVs away from the active zone may lead to their increase in size and irregular shape.

Our NMR structural analysis allows the study of proteins within intact synapses derived directly from animals. This approach revealed features of how αSyn behaves in its native environment that have not been heretofore reported (Figure 4). We show that these changes appear to be independent of hydrogen exchange (Figure S4) and molecular crowding (Figure S5). Furthermore, although high local concentrations of Ca^{2+} led to spectrometric changes in the C-terminal region of both WT and 3K αSyn, an overall ~70% loss of NMR signal intensity in the N-terminal region (residues 3–100) occurred only when WT αSyn was electroporated inside synaptosomes. We speculate that this NMR signal intensity loss results from transient protein-protein interactions (potentially including multimer formation of the electroporated αSyn, as demonstrated in Figure 5) as well as protein-membrane interactions taking place between the exogenous αSyn and the intact intra-synaptosomal milieu. Some of these NMR signatures are also in line with αSyn's recently reported interactions with chaperones such as HSC70 and HSP90 (Burmann et al., 2020). The overall attenuation of its NMR signal is also consistent with *in vitro* reports in which proteins that experience phase separation undergo significant reductions in their NMR signal intensity (Kim et al., 2019), a

proposed mechanism of synaptic function (Milovanovic et al., 2018). We also describe large C-terminal CSPs consistent with the previously reported Ca^{2+} binding (Lautenschläger et al., 2018) that are abolished with chelating agents without affecting NMR signal attenuation (Figure S6).

Although we are unable to directly detect NMR signatures interpretable as coming from folded, bound, or multimeric αSyn species, the consistent signal attenuation we see suggests that the soluble, monomeric species, while detectable, is significantly less prevalent within synaptosomes than it is in aqueous buffer, where close to 100% of αSyn exists as unfolded monomers (Fonseca-Ornelas et al., 2017). We hypothesize that the formation of αSyn multimers could be the primary explanation behind such signal attenuation, rather than membrane binding, since the broadening of NMR signals is not limited to the first ~40 residues of αSyn (Figure 4F), where membrane recognition and binding primarily occur (Fusco et al., 2014). Additionally, we were able to cross-link multimers of exogenous αSyn inside the synaptosomes (Figure 5F, higher molecular weight [MW] bands). Interestingly, the amount of NMR signal we observe inside synaptosomes (which comes from monomeric, soluble, and unfolded species) is higher for the 3K variant, particularly in its NAC domain (Figure 4E), and this is accompanied by a significantly reduced level of DSG-trapped multimeric species in the 3K than the WT αSyn (Figures 5F and 5H). This result also suggests that more 3K molecules have an exposed NAC domain, leaving it susceptible to initiate deleterious nucleation processes that lead to αSyn aggregation *in vivo*. Notably, the proportion of signal attenuation of αSyn inside synaptosomes due to membrane binding is likely to be different for the WT and 3K variants, as the 3K αSyn has a higher affinity for membranes and should therefore have a less intense NMR signal than the WT variant (Dettmer et al., 2015b; Imberdis et al., 2019; Nuber et al., 2018). The spectral changes we observed in the N-terminal region of WT and less so 3K in intact synaptosomes are largely abolished by synaptosome lysis via sonication (Figure S6), suggesting that not only the presence of synaptosomal biochemical components but also their proper physiological localization and local concentrations within intact synaptosomes are necessary for the native conformational dynamics of αSyn.

Inside synaptosomes, we observed significantly less pronounced NMR signal attenuation of recombinant αSyn in the absence of endogenous mouse αSyn (Figures 5C–5E). Since we also observed fewer DSG-trapped multimers of recombinant αSyn in αSyn-KO synaptosomes (Figures 5G and 5H), we speculate that the physiologic multimerization of exogenous αSyn is regulated not only by its sequence and its transient interaction with cellular components in the synapse that could function as cofactors (e.g., small molecules and free lipids [Dettmer et al., 2013]) but also by interactions with already folded endogenous αSyn. Without the “priming” provided by endogenous αSyn, the recombinant αSyn alone, while still able to transiently bind Ca^{2+} and other synaptosomal components in its C-terminal region (Figure 5E), fails to undergo multimerization (Figures 5E, 5G, and 5H). In this regard, we propose that the formation of native multimers on vesicles, perhaps followed by their partial detachment and presence in the cytosol, is a normal physiological property of αSyn (Rovere et al., 2018a), and the decrease of native tetramers in intact neurons has been directly shown to compromise the known αSyn-mediated vesicle trafficking function of αSyn (Wang et al., 2014). Because the *in vitro* aggregation profiles

of the WT, E46K, and 3K variants of αSyn were not significantly different from each other (Figure S1B), we speculate that the effects that we observe at synapses *in vivo* are related to changes in the function and networking of αSyn, rather than to enhanced aggregation.

In Figure 6, we summarize our hypothetical model based on the findings herein. We conclude that the intact synaptosomal compartment, by means of its high ion concentration as well as the molecular crowding of proteins, lipids, and membranes, mediates the reshaping of the conformational dynamics and interaction network of the initially "natively unfolded" recombinant WT αSyn monomers. The E46K-related 3K variant is unable to undergo this process because of the E→K mutations, which both lower tetramer/multimer propensity and increase membrane binding that together hinder the necessary dynamic equilibrium of αSyn. We were not able to detect these differences in previous NMR studies performed in aqueous buffer (Rovere et al., 2019), highlighting the power of our approach based on the introduction of a synaptic protein into a physiologically relevant microenvironment. Nevertheless, our study has limitations. The nature of our intra-synaptosome sample (very low concentration of NMR-visible protein and short viability period) does not yet lend itself to the kinds of experiments that could potentially shed light on the structural features of the conformations that αSyn adopts inside synaptosomes. For example, multidimensional carbon-coupled, diffusion or spin-relaxation experiments demand munch longer experimental times and higher protein concentrations. Despite this shortcoming, our NMR synaptosome approach highlights the importance of attempting to bridge the gap between biophysics (in vitro) and cell biology (in vivo). With the advance of techniques such as cryo-electron tomography, in-cell single-molecule fluorescence resonance energy transfer (FRET), and in-cell NMR (Plitzko et al., 2017), in situ approaches like the one presented here will potentially address critical questions about the physiology of proteins like αSyn, which show diverse and dynamic conformations in their native, highly complex environments.

STAR★METHODS

RESOURCE AVAILABILITY

Lead contact—Further information and requests for resources and reagents should be directed to and will be fulfilled by the Lead Contact, Dennis J. Selkoe (dselkoe@bwh.harvard.edu).

Materials availability—This study did not generate new unique reagents.

Data and code availability—This study did not generate any unique datasets or code.

EXPERIMENTAL MODEL AND SUBJECT DETAILS

C57BL6;Tg(SNCA*E35K-E46K-E61K)3KL-3798 (homozygous), B6N.Cg-Tg (SNCA*E46K) 3Elan/J (heterozygous), C57BL6;Tg (SNCA*WT)WT-3877 (heterozygous), C57BL/6NCrl, and C57BL/6NTac SNCA KO (homozygous) mice were either purchased from The Jackson Laboratory (E46K: JAX #018768; JAX: 3KL-032799)Charles River (C57Bl6; #027) or generated in house (Line WT-3877). All mice lines were

immunocompetent and were housed under standard specific pathogen-free conditions and maintained at the Hale BTM facility in accordance with National Institutes of Health guidelines on use of laboratory animals and an approved protocol by the Brigham and Women's Hospital (IACUC protocol #2016000314). Mice were kept in normal 12 h light/12 h dark cycles and had free access to food and water. Because of the selective more relevant phenotype that we have previously observed in $3KL^{+/+}$ (Fanning et al., 2019; Nuber et al., 2018; Rajsombath et al., 2019), all mice in this study were males and age matched at 12 months.

METHOD DETAILS

Synaptosome preparation—Synaptosomes were purified from brain tissue harvested from mice of the denoted genotypes according to previously described methods (Dunkley et al., 2008; Fernández-Busnadiego, 2018) following the Harvard Medical School Committee on Animals guidelines. Briefly, mice of around 12 months of age were selected, and, after administration of anesthesia, animals of the specified genotypes were decapitated, their brains harvested, and the cerebella discarded. Brain tissue was homogenized in 4 mL (10% w/v) of homogenization buffer (HB; 0.32 M sucrose, 4 mM HEPES, 20 mM DTT, 50 mM EDTA, protease inhibitor cocktail (Roche, Branchburg, NJ), pH 7.4) with seven slow and uniform strokes at ~600 rpm in a Potter-Elvehjem homogenizer. The resulting homogenate was centrifuged for 5 minutes at 1000×*g*, and the pellet discarded. The supernatant (total homogenate fraction) was centrifuged at 14500×*g* for 12 minutes. The resulting supernatant was named "cytosolic fraction," and the pellet was resuspended in HB and loaded on top of a three-step (3%, 10%, and 23%) Percoll gradient (Sigma Aldrich, Natick, MA). After a 12-minute centrifugation step at 18700*xg* in an SS34 bucket rotor (Thermo Fisher, Waltham, MA), the synaptosome-rich interface between 10% and 23% Percoll was recovered using a glass Pasteur pipette. To remove the Percoll from the isolated fraction, the sample was resuspended in a 30-mL volume of Saline Buffer (SB; 0.32 M sucrose, 140 mM NaCl, 5 mM KCl, 5 mM $NaHCO_3$, 1.2 mM NaH_2PO_4, 1 mM MgCl, 20 mM HEPES pH 7.4 *or* 6.6, depending on the particular experiment) and centrifuged at 18700*xg* for 12 minutes. The supernatant was discarded, and the synaptosomal pellet resuspended in enough saline buffer to obtain a final protein concentration of ~1 mg/mL.

Western blotting—For western blotting, 10 μg of total protein were boiled for 10 minutes at 100°C, loaded on a 4%–12% Bis-Tris gel (Invitrogen, Carlsbad, CA) and transferred to nitrocellulose membranes using the default, 7-minute iBlot protocol (Invitrogen, Carlsbad, CA). After the transfer, membranes were fixed in 0.4% paraformaldehyde (PFA) for 20 minutes and then blocked for 1 hour at room temperature using Odyssey Blocking Buffer (LI-COR Biotechnology, Lincoln, NE). Blots were then incubated overnight with the selected primary antibodies, washed with PBS-T, and incubated for 45 minutes with infrared secondary antibodies (LI-COR Biotechnology, Lincoln, NE). For SDS-resistant SNARE-complex assembly quantification, samples were not boiled and immediately loaded on the gel. The SDS-resistant SNARE-complexes were defined as the immunoreactive bands larger than ~40 kDa that were absent in the boiled samples. All densitometries were performed with the ImageStudio software (LI-COR Biotechnology, Lincoln, NE).

Immunofluorescence—A synaptosomal solution at 0.1 mg/mL concentration in SB was allowed to bind to poly-D-lysine-coated coverslips overnight at 4°C. After two 5-minutes washes with HBSS to remove unattached synaptosomes, the sample was fixed with 4% (w/v) paraformaldehyde for 15 minutes, washed twice with PBS, permeabilized in PBS with 0.3% Triton X-100 for 10 minutes, and blocked for 1 h in PBS-T with 5% (w/v) non-fat milk. Coverslips were incubated with primary antibody overnight, washed twice for 5 minutes, and then labeled with either Alexa Fluor-568 (red) anti-rabbit or Alexa Fluor-488 (green) anti-mouse secondary antibodies for 1 h at room temperature. After washing, the preparations were visualized in a Carl-Zeiss LSM710 confocal microscope (acquisition software: Zen, Carl-Zeiss, White Plain, NY).

Electron microscopy—Fresh synaptosomes from the denoted genotypes were pelleted at ~5000×g for 10 minutes. The pellet was then fixed with a solution of 2.5% Glutaraldehyde 1.25% paraformaldehyde and 0.03% picric acid in 0.1 M sodium cacodylate buffer (pH 7.4) overnight. The pellets were washed in 0.1M cacodylate buffer and postfixed with 1% osmium tetroxide (OsO_4)/1.5% potassium ferrocyanide ($KFeCN_6$) for 1 hour, washed 2x in water, 1x maleate buffer (MB) 1x and incubated in 1% uranyl acetate in MB for 1hr followed by 2 washes in water and subsequent dehydration in grades of alcohol. The samples were then put in propyleneoxide for 1 hr and infiltrated overnight in a 1:1 mixture of propyleneoxide and TAAB Epon (TAAB Laboratories Equipment Ltd, Reading, UK). The following day the samples were embedded in TAAB Epon and polymerized at 60°C for 48 hr. Ultrathin sections (about 60nm) were cut on a Reichert Ultracut-S microtome, picked up on to copper grids, stained with lead citrate and examined in a TecnaiG^2 Spirit BioTWIN (Thermo Fisher, Waltham, MA). Images were recorded with an AMT 2k CCD camera (AMT, Woburn, MA). The presence of recombinant αSyn inside the synaptosomes was probed with immunogold electron microscopy; after etching the Epon sections in a solution of saturated solution of sodium metaperiodate in water for 5 min at RT grids were washed 3x in water and floated on 0.1% Triton X-100 for 5 min at RT. Blocking was carried out using 1% BSA + 0.1% TX-100/PBS for 1 hr at RT. Grids were incubated with anti-αS antibody 4B12 (1:50) in 1% BSA + 0.1% TX-100/PBS overnight at 4°C. Grids were washed four times in PBS followed by incubation with rabbit-anti-mouse bridging antibody (1:50) (ab6709 Abcam, Cambridge, MA) for 1 hr at RT, washed again four times in PBS and incubated in 15 nm Protein A-gold particles (Department of cell biology, University Medical Center Utrecht, the Netherlands) for 30 minutes at RT. Grids were finally washed with PBS and water, stained with lead citrate and imaged as above. Morphometric analysis for number, size, and shape of SVs was blind to genotype. For ultrastructural analysis, a minimum of 20 images per mouse genotype were evaluated in a blinded fashion.

FM 2–10 dye uptake and release assay—Freshly-prepared synaptosome suspensions (600 μg of total synaptosomal protein in 500 μL of calcium-containing HBSS) were incubated with 100 μM of FM 2–10 Dye (Sigma Aldrich, Natick, MA) at room temperature. To stimulate the uptake of the dye, the synaptosomes were incubated with 30 mM KCl. After 15 minutes at room temperature to allow dye internalization, synaptosomes were pelleted by centrifuging for 5 minutes at 15000×*g* and washed twice with HBSS to remove excess, non-internalized dye. Synaptosomes were then resuspended in HBSS either with

or without 1.2 mM $CaCl_2$. The release of the dye was induced with 30 mM KCl and monitored in a POLARstar Omega plate reader (BMG Labtech, Ortenberg, Germany) at Ex/Em 506/620nm for 30 minutes.

15N- or 15N13C-labeled protein expression—For the expression of ^{15}N- or $^{15}N^{13}C$-labeled human WT αSyn and its 3K variant, the bacteria were grown in M9 complete medium+ampicillin, supplemented with $^{15}NH_4Cl$ and ^{13}C-D-glucose. M9 complete medium was prepared fresh from a 10x M9 medium stock (60 g/L Na_2HPO_4, 30 g/L KH_2PO_4, 5 g/L NaCl), 50× 20% D-glucose, 1000× 1 M $MgSO_4$, 5000× 1 M $CaCl_2$, 1000× 1 mg/mL thiamine and biotin, 100x trace element solution, 1000x vitamin solution and 1 g/L $^{15}NH_4Cl$. The 100x trace element solution was prepared by dissolving (in 1 L MilliQ water) 5 g ethylenediaminetetraacetic acid (EDTA), 0.50 g $FeCl_3$, 84 mg $ZnCl_2$, 12 mg $CuSO_4$, 10 mg $CoCl_2 \cdot 6H_2O$, 10 mg H_3BO_3, 1.6 mg $MnCl_2 \cdot 4H_2O$, 1.6 mg $Na_2MoO_4 \cdot 2H_2O$, and adjusting the pH to 7.0 (it was then filter-sterilized and stored at RT). The 1000x vitamin solution was prepared by dissolving (in 1 L 95% MilliQ water, 5% acetonitrile), 50 mg riboflavin, 0.5 g niacinamide, 0.5 g pyridoxine hydrochloride, 0.5 g thiamine. After filtration with a 0.22-μm cutoff (to sterilize and remove the undissolved riboflavin), the solution was stored at 4°C, protected from light. BL21(DE3) *E. coli* (New England Biolabs, Ipswich, MA) were cotransformed with the pET21a-based constructs (a kind gift from the Michael J. Fox Foundation MJFF (Addgene plasmid # 51486), and pTSara-NatB for N-terminally acetylated αSyn (Johnson et al., 2010; Rovere et al., 2018b). Cultures were grown for 6–8 hr at 37°C under shaking, then used to inoculate an overnight pre-culture in M9 complete medium+ampicillin, which, on the following day, was diluted again 1:10 in M9 complete medium+ampicillin. Cultures were induced at an OD_{600} of ~0.5 with 1 mM isopropyl-β-D-thiogalactopyranoside (IPTG) for 4 hr. The cell pellet, after harvesting, was resuspended in 20 mM Tris buffer, 25 mM NaCl, pH 8.0, and lysed by boiling for 15 minutes The supernatant of a 20-minute, 20000*xg* spin of the lysate was then further processed. The sample was loaded on two 5-mL (tandem) HiTrap Q HP anion exchange columns (GE Healthcare, Pittsburgh, PA), equilibrated with 20 mM Tris buffer, 25 mM NaCl, pH 8.0. αSyn was eluted from the columns with a 25–1000 mM NaCl gradient of 20 mM Tris buffer, 1 M NaCl, pH 8.00. Peak fractions were pooled and further purified via gel filtration on a HiPrep Sephacryl S-200 HR 16/60 gel filtration column (GE Healthcare, Pittsburgh, PA) using 50 mM NH_4Ac, pH 7.40 as running buffer. Peak fractions (> 95% pure, as estimated by Coomassie Brilliant Blue-stained SDS-PAGE) were pooled, aliquoted, lyophilized, and stored at −20°C. Purified samples were also analyzed by Matrix-Assisted Laser Desorption Ionization-Time Of Flight (MALDI-TOF) Mass Spectrometry (MS) and trypsin digestion followed by MALDI-TOF MS, to confirm the intact mass, the isotopic enrichment, and the sequence of the proteins (Molecular Biology Core Facilities, Dana-Farber Cancer Institute). Lyophilized proteins were reconstituted fresh, before experiments, in saline buffer, pH 7.4 to 6.6, and never reused. Protein solutions were spun down every time after resuspension, before spectroscopic quantitation of the protein concentration, at 21130*xg* for 20 minutes at 4°C, to remove any large αSyn aggregates. Concentration was quantified by measuring the absorbance at 280 nm (ε = 0.412 mg/mL·cm).

Protein electroporation and NMR—~800-μM samples of either ^{15}N or $^{15}N^{13}C$-labeled WT or 3K αSyn were added to a suspension of synaptosomes with a concentration of ~8 mg/mL (total protein) in 400 μL of saline buffer (0.32 M sucrose, 140 mM NaCl, 5 mM KCl, 5 mM $NaHCO_3$, 1.2 mM NaH_2PO_4, 1 mM MgCl, 20 mM HEPES, pH ranged from 7.4 to 6.6, depending on the particular experiment) containing 2 mM ATP (Thermo Fisher, Waltham, MA) and 2 mM reduced glutathione (Sigma Aldrich, Natick, MA). The sample was then split into four 100 μL aliquots then transferred to 2-mm electroporation cuvettes for the Amaxa Nucleofector (Lonza, Walkersville, MD). The program code was EA100, and two pulses were used, with gentle mixing between them. Immediately after the electroporation, the synaptosomal solution was pelleted for 10 minutes at 5000×*g* to discard the supernatant containing all the recombinant protein that was not delivered inside the synaptosomes. The pellet was then resuspended in sodium carbonate buffer at pH 11.0 to remove all the proteins attached to the plasma membrane, pelleted again, and subjected to a 0.01% trypsin treatment for 45 s at room temperature to cleave non-internalized protein, followed by one final wash with saline buffer (see above). The concentration of internalized αSyn was determined by semiquantitative western blot, as described previously (Theillet et al., 2016). Briefly, aliquots of the NMR samples used in the experiments were loaded on an SDS-PAGE gel. These aliquots represented either 100% (undiluted) or 50%, 25%, or 12.5% (diluted) of the corresponding NMR spectra. By comparing them to a dilution series of recombinant αSyn loaded on the same gel, we were able to estimate the concentration of αSyn present inside the synaptosomes. We used the αSyn antibody 4B12, which recognizes only human αSyn, to ensure that the murine, NMR-invisible αSyn did not contribute to our estimates. ^{1}H-^{15}N HSQC spectra of ^{15}N-labeled WT or 3K αSyn were recorded directly after the washes with the addition of 10% D_2O in a 5-mm NMR tube. The final NMR buffer was 0.32 M sucrose, 140 mM NaCl, 5 mM KCl, 5 mM $NaHCO_3$, 1.2 mM NaH_2PO_4, 1 mM MgCl, 20 mM HEPES pH 7.4 *or* 6.6, according to the particular experiment. Spectra were recorded on a 600 MHz Bruker AVANCE II spectrometer (Bruker, Billerica, MA) equipped with a Prodigy CryoProbe, at 15°C and using 25% NUS sampled using Poisson Gap distribution and reconstructed using the hmsIST protocol (Hyberts et al., 2012). Resonances were assigned, where possible, by inspection and comparison with the previously assigned spectra of WT αSyn (BRMB 6968 and 5744). SOFAST experiments were acquired on a Bruker Avance III spectrometer operating at 800 MHz equipped with a TXO cryoprobe. The SOFAST ^{13}C-HMQC pulse sequence using constant time homonuclear decoupling was used, as reported in (Amero et al., 2009). Selective 90° excitation was achieved using a pc9_4_90.1000 pulse shape, and selective water flip-back using Rsnob.1000. Carrier frequencies were set to 1 ppm for ^{1}H and 17 ppm for ^{13}C. The recycle delay was set to 0.2 s.

Thioflavin T fluorescence assay—Solutions of WT, E46K, and 3K αSyn variants at 50 μM were incubated in the presence of 0.01% NaN_3 and aggregation was monitored using a continuous ThT assay. Six replicates (100 μL each) were transferred to non-binding, black, clear bottom, half-area non-treated 96-well plates (Corning Life Sciences, Corning, NY). Reactions prepared in the absence of recombinant protein were included as blanks to subtract basal ThT fluorescence. Plates were covered with adhesive plate sealers (VWR, Radnor, PA) and incubated at 37°C in a POLARstar Omega plate reader (BMG Labtech, Ortenberg, Germany) with shaking at 100 RPM for 300 s before each reading. Fluorescence

was recorded every 10 minutes (Excitation: 440 nm, Emission: 480 nm) and assays were carried on for at least 96 hr.

QUANTIFICATION AND STATISTICAL ANALYSIS

All statistical analysis was performed in GraphPad Prism versions 8 and 9. Where applicable data was first tested for normality using a D'Agostino-Pearson test. In all the studied cases, our data followed a Gaussian distribution. Tests used and n values for number of baseline mice, images, or NMR references are included in the individual figure legends, as well as in the results section. Data is shown as SD or as SEM where appropriate. Sidak's correction for multiple comparisons was used also where appropriate. As stated in the figure legends, standard symbols indicate *$p < 0.05$, **$p < 0.01$, ***$p < 0.001$, ****$p < 0.0001$.

NMR data processing and analysis—Data processing and analysis were performed with the Bruker TopSpin software and CcpNmr Analysis (Vranken et al., 2005). Perturbations in the chemical shift values for ^{1}H and ^{15}N were calculated as $[(\Delta\delta^{1}H)^{2}+(0.15\cdot\Delta\delta^{15}N)^{2}]^{1/2}$.

Supplementary Material

Refer to Web version on PubMed Central for supplementary material.

ACKNOWLEDGMENTS

We thank the members of the Selkoe, Dettmer, and Bartels labs for helpful discussions. This work was supported by NIH grants R01 NS109510 (S.N.) and R01 NS083845 (D.J.S.).

REFERENCES

Alex A, Piano V, Polley S, Stuiver M, Voss S, Ciossani G, Overlack K, Voss B, Wohlgemuth S, Petrovic A, et al. (2019). Electroporated recombinant proteins as tools for in vivo functional complementation, imaging and chemical biology. eLife 8, e48287. [PubMed: 31310234]

Amero C, Schanda P, Durá MA, Ayala I, Marion D, Franzetti B, Brutscher B, and Boisbouvier J (2009). Fast two-dimensional NMR spectroscopy of high molecular weight protein assemblies. J. Am. Chem. Soc. 131, 3448–3449. [PubMed: 19243101]

Atias M, Tevet Y, Sun J, Stavsky A, Tal S, Kahn J, Roy S, and Gitler D (2019). Synapsins regulate α-synuclein functions. Proc. Natl. Acad. Sci. USA 116, 11116–11118. [PubMed: 31110014]

Baldwin ML, Rostas JAP, and Sim ATR (2003). Two modes of exocytosis from synaptosomes are differentially regulated by protein phosphatase types 2A and 2B. J. Neurochem. 85, 1190–1199. [PubMed: 12753078]

Bartels T, Choi JG, and Selkoe DJ (2011). α-Synuclein occurs physiologically as a helically folded tetramer that resists aggregation. Nature 477, 107–110. [PubMed: 21841800]

Bertoncini CW, Jung Y-S, Fernandez CO, Hoyer W, Griesinger C, Jovin TM, and Zweckstetter M (2005). Release of long-range tertiary interactions potentiates aggregation of natively unstructured α-synuclein. Proc. Natl. Acad. Sci. USA 102, 1430–1435. [PubMed: 15671169]

Binolfi A, Limatola A, Verzini S, Kosten J, Theillet F-X, Rose HM, Bekei B, Stuiver M, van Rossum M, and Selenko P (2016). Intracellular repair of oxidation-damaged α-synuclein fails to target C-terminal modification sites. Nat. Commun. 7, 10251. [PubMed: 26807843]

Burmann BM, Gerez JA, Matečko-Burmann I, Campioni S, Kumari P, Ghosh D, Mazur A, Aspholm EE, Šulskis D, Wawrzyniuk M, et al. (2020). Regulation of α-synuclein by chaperones in mammalian cells. Nature 577, 127–132. [PubMed: 31802003]

Burré J, Sharma M, Tsetsenis T, Buchman V, Etherton MR, and Südhof TC (2010). α-Synuclein promotes SNARE-complex assembly in vivo and in vitro. Science 329, 1663–1667. [PubMed: 20798282]

Burré J, Sharma M, and Südhof TC (2012). Systematic mutagenesis of α-synuclein reveals distinct sequence requirements for physiological and pathological activities. J. Neurosci. 32, 15227–15242. [PubMed: 23100443]

Burré J, Sharma M, and Südhof TC (2014). α-Synuclein assembles into higher-order multimers upon membrane binding to promote SNARE complex formation. Proc. Natl. Acad. Sci. USA 111, E4274–E4283. [PubMed: 25246573]

Clayton DF, and George JM (1998). The synucleins: a family of proteins involved in synaptic function, plasticity, neurodegeneration and disease. Trends Neurosci. 21, 249–254. [PubMed: 9641537]

Cote Y, Delarue P, Scheraga HA, Senet P, and Maisuradze GG (2018). From a highly disordered to a metastable state: uncovering insights of α-synuclein. ACS Chem. Neurosci. 9, 1051–1065. [PubMed: 29451381]

Davidson WS, Jonas A, Clayton DF, and George JM (1998). Stabilization of α-synuclein secondary structure upon binding to synthetic membranes. J. Biol. Chem. 273, 9443–9449. [PubMed: 9545270]

Dettmer U, Newman AJ, Luth ES, Bartels T, and Selkoe D (2013). In vivo cross-linking reveals principally oligomeric forms of α-synuclein and β-synuclein in neurons and non-neural cells. J. Biol. Chem. 288, 6371–6385. [PubMed: 23319586]

Dettmer U, Newman AJ, Soldner F, Luth ES, Kim NC, von Saucken VE, Sanderson JB, Jaenisch R, Bartels T, and Selkoe D (2015a). Parkinson-causing α-synuclein missense mutations shift native tetramers to monomers as a mechanism for disease initiation. Nat. Commun. 6, 7314. [PubMed: 26076669]

Dettmer U, Newman AJ, von Saucken VE, Bartels T, and Selkoe D (2015b). KTKEGV repeat motifs are key mediators of normal α-synuclein tetramerization: their mutation causes excess monomers and neurotoxicity. Proc. Natl. Acad. Sci. USA 112, 9596–9601. [PubMed: 26153422]

Dettmer U, Selkoe D, and Bartels T (2016). New insights into cellular α-synuclein homeostasis in health and disease. Curr. Opin. Neurobiol. 36, 15–22. [PubMed: 26282834]

Dettmer U, Ramalingam N, von Saucken VE, Kim T-E, Newman AJ, Terry-Kantor E, Nuber S, Ericsson M, Fanning S, Bartels T, et al. (2017). Loss of native α-synuclein multimerization by strategically mutating its amphipathic helix causes abnormal vesicle interactions in neuronal cells. Hum. Mol. Genet. 26, 3466–3481. [PubMed: 28911198]

Deutsch C, Drown C, Rafalowska U, and Silver IA (1981). Synaptosomes from rat brain: morphology, compartmentation, and transmembrane pH and electrical gradients. J. Neurochem. 36, 2063–2072. [PubMed: 7241148]

Deutsch C, Taylor JS, and Wilson DF (1982). Regulation of intracellular pH by human peripheral blood lymphocytes as measured by 19F NMR. Proc. Natl. Acad. Sci. USA 79, 7944–7948. [PubMed: 6961462]

Dunkley PR, Jarvie PE, and Robinson PJ (2008). A rapid Percoll gradient procedure for preparation of synaptosomes. Nat. Protoc. 3, 1718–1728. [PubMed: 18927557]

Evans GJO (2015). The synaptosome as a model system for studying synaptic physiology. Cold Spring Harb. Protoc. 2015, 421–424. [PubMed: 25934942]

Fanning S, Haque A, Imberdis T, Baru V, Barrasa MI, Nuber S, Termine D, Ramalingam N, Ho GPH, Noble T, et al. (2019). Lipidomic analysis of α-synuclein neurotoxicity identifies stearoyl CoA desaturase as a target for Parkinson treatment. Mol. Cell 73, 1001–1014.e8. [PubMed: 30527540]

Fernández-Busnadiego R (2018). Cryo-electron tomography of the mammalian synapse. Methods Mol. Biol. 1847, 217–224. [PubMed: 30129020]

Flagmeier P, Meisl G, Vendruscolo M, Knowles TPJ, Dobson CM, Buell AK, and Galvagnion C (2016). Mutations associated with familial Parkinson's disease alter the initiation and amplification steps of α-synuclein aggregation. Proc. Natl. Acad. Sci. USA 113, 10328–10333. [PubMed: 27573854]

Fonseca-Ornelas L, Eisbach SE, Paulat M, Giller K, Fernández CO, Outeiro TF, Becker S, and Zweckstetter M (2014). Small molecule-mediated stabilization of vesicle-associated helical α-

synuclein inhibits pathogenic misfolding and aggregation. Nat. Commun. 5, 5857. [PubMed: 25524885]

Fonseca-Ornelas L, Schmidt C, Camacho-Zarco AR, Fernandez CO, Becker S, and Zweckstetter M (2017). Small-molecule-induced soluble oligomers of α-synuclein with helical structure. Chemistry 23, 13010–13014. [PubMed: 28763125]

Fortin DL, Troyer MD, Nakamura K, Kubo S, Anthony MD, and Edwards RH (2004). Lipid rafts mediate the synaptic localization of α-synuclein. J. Neurosci. 24, 6715–6723. [PubMed: 15282274]

Fortin DL, Nemani VM, Voglmaier SM, Anthony MD, Ryan TA, and Edwards RH (2005). Neural activity controls the synaptic accumulation of α-synuclein. J. Neurosci. 25, 10913–10921. [PubMed: 16306404]

Fujishiro H, Imamura AY, Lin W-L, Uchikado H, Mark MH, Golbe LI, Markopoulou K, Wszolek ZK, and Dickson DW (2013). Diversity of pathological features other than Lewy bodies in familial Parkinson's disease due to SNCA mutations. Am. J. Neurodegener. Dis. 2, 266–275. [PubMed: 24319644]

Fusco G, De Simone A, Gopinath T, Vostrikov V, Vendruscolo M, Dobson CM, and Veglia G (2014). Direct observation of the three regions in α-synuclein that determine its membrane-bound behaviour. Nat. Commun. 5, 3827. [PubMed: 24871041]

Fusco G, Pape T, Stephens AD, Mahou P, Costa AR, Kaminski CF, Kaminski Schierle GS, Vendruscolo M, Veglia G, Dobson CM, and De Simone A (2016). Structural basis of synaptic vesicle assembly promoted by α-synuclein. Nat. Commun. 7, 12563. [PubMed: 27640673]

George JM, Jin H, Woods WS, and Clayton DF (1995). Characterization of a novel protein regulated during the critical period for song learning in the zebra finch. Neuron 15, 361–372. [PubMed: 7646890]

Giasson BI, Murray IV, Trojanowski JQ, and Lee VM (2001). A hydrophobic stretch of 12 amino acid residues in the middle of α-synuclein is essential for filament assembly. J. Biol. Chem. 276, 2380–2386. [PubMed: 11060312]

Hyberts SG, Milbradt AG, Wagner AB, Arthanari H, and Wagner G (2012). Application of iterative soft thresholding for fast reconstruction of NMR data non-uniformly sampled with multidimensional Poisson gap scheduling. J. Biomol. NMR 52, 315–327. [PubMed: 22331404]

Imberdis T, Negri J, Ramalingam N, Terry-Kantor E, Ho GPH, Fanning S, Stirtz G, Kim T-E, Levy OA, Young-Pearse TL, et al. (2019). Cell models of lipid-rich α-synuclein aggregation validate known modifiers of α-synuclein biology and identify stearoyl-CoA desaturase. Proc. Natl. Acad. Sci. USA 116, 20760–20769. [PubMed: 31548371]

Jo E, McLaurin J, Yip CM, St George-Hyslop P, and Fraser PE (2000). alpha-Synuclein membrane interactions and lipid specificity. J. Biol. Chem. 275, 34328–34334. [PubMed: 10915790]

Johnson M, Coulton AT, Geeves MA, and Mulvihill DP (2010). Targeted amino-terminal acetylation of recombinant proteins in *E. coli*. PLoS ONE 5, e15801. [PubMed: 21203426]

Kim S, Yun SP, Lee S, Umanah GE, Bandaru VVR, Yin X, Rhee P, Karuppagounder SS, Kwon S-H, Lee H, et al. (2018). GBA1 deficiency negatively affects physiological α-synuclein tetramers and related multimers. Proc. Natl. Acad. Sci. USA 115, 798–803. [PubMed: 29311330]

Kim TH, Tsang B, Vernon RM, Sonenberg N, Kay LE, and Forman-Kay JD (2019). Phospho-dependent phase separation of FMRP and CAPRIN1 recapitulates regulation of translation and deadenylation. Science 365, 825–829. [PubMed: 31439799]

Kohl Z, Ben Abdallah N, Vogelgsang J, Tischer L, Deusser J, Amato D, Anderson S, Müller CP, Riess O, Masliah E, et al. (2016). Severely impaired hippocampal neurogenesis associates with an early serotonergic deficit in a BAC α-synuclein transgenic rat model of Parkinson's disease. Neurobiol. Dis. 85, 206–217. [PubMed: 26523794]

Lautenschläger J, Stephens AD, Fusco G, Ströhl F, Curry N, Zacharopoulou M, Michel CH, Laine R, Nespovitaya N, Fantham M, et al. (2018). C-terminal calcium binding of α-synuclein modulates synaptic vesicle interaction. Nat. Commun. 9, 712. [PubMed: 29459792]

Logan T, Bendor J, Toupin C, Thorn K, and Edwards RH (2017). α-Synuclein promotes dilation of the exocytotic fusion pore. Nat. Neurosci. 20, 681–689. [PubMed: 28288128]

Man WK, Tahirbegi B, Vrettas MD, Preet S, Ying L, Vendruscolo M, De Simone A, and Fusco G (2021). The docking of synaptic vesicles on the presynaptic membrane induced by α-synuclein is modulated by lipid composition. Nat. Commun. 12, 927. [PubMed: 33568632]

Medeiros AT, Soll LG, Tessari I, Bubacco L, and Morgan JR (2017). α-Synuclein dimers impair vesicle fission during clathrin-mediated synaptic vesicle recycling. Front. Cell. Neurosci. 11, 388. [PubMed: 29321725]

Milovanovic D, Wu Y, Bian X, and De Camilli P (2018). A liquid phase of synapsin and lipid vesicles. Science 361, 604–607. [PubMed: 29976799]

Minton AP (2001). The influence of macromolecular crowding and macromolecular confinement on biochemical reactions in physiological media. J. Biol. Chem. 276, 10577–10580. [PubMed: 11279227]

Nachshen DA, and Drapeau P (1988). The regulation of cytosolic pH in isolated presynaptic nerve terminals from rat brain. J. Gen. Physiol. 91, 289–303. [PubMed: 3373180]

Nemani VM, Lu W, Berge V, Nakamura K, Onoa B, Lee MK, Chaudhry FA, Nicoll RA, and Edwards RH (2010). Increased expression of α-synuclein reduces neurotransmitter release by inhibiting synaptic vesicle reclustering after endocytosis. Neuron 65, 66–79. [PubMed: 20152114]

Nishida A, Iwata H, Kudo Y, Kobayashi T, Matsuoka Y, Kanai Y, and Endou H (2004). Measurement of glutamate uptake and reversed transport by rat synaptosome transporters. Biol. Pharm. Bull. 27, 813–816. [PubMed: 15187424]

Nuber S, Rajsombath M, Minakaki G, Winkler J, Müller CP, Ericsson M, Caldarone B, Dettmer U, and Selkoe DJ (2018). Abrogating native α-synuclein tetramers in mice causes a L-DOPA-responsive motor syndrome closely resembling Parkinson's disease. Neuron 100, 75–90.e5. [PubMed: 30308173]

Nussbaum RL (2016). The identification of alpha-synuclein as the first Parkinson disease gene. J. Parkinsons Dis. 7, S43–S49.

Perrin RJ, Woods WS, Clayton DF, and George JM (2001). Exposure to long chain polyunsaturated fatty acids triggers rapid multimerization of synucleins. J. Biol. Chem. 276, 41958–41962. [PubMed: 11553616]

Plitzko JM, Schuler B, and Selenko P (2017). Structural biology outside the box-inside the cell. Curr. Opin. Struct. Biol. 46, 110–121. [PubMed: 28735108]

Rajsombath MM, Nam AY, Ericsson M, and Nuber S (2019). Female sex and brain-selective estrogen benefit α-synuclein tetramerization and the PD-like motor syndrome in 3K transgenic mice. J. Neurosci. 39, 7628–7640. [PubMed: 31405930]

Ramanathan M, Kuo H-R, Lambert CW, and Ingoglia NA (2000). Introduction of macromolecules into synaptosomes using electroporation. J. Neurosci. Methods 96, 19–23. [PubMed: 10704667]

Rizzoli SO, and Betz WJ (2004). The structural organization of the readily releasable pool of synaptic vesicles. Science 303, 2037–2039. [PubMed: 15044806]

Rovere M, Sanderson JB, Fonseca-Ornelas L, Patel DS, and Bartels T (2018a). Refolding of helical soluble α-synuclein through transient interaction with lipid interfaces. FEBS Lett. 592, 1464–1472. [PubMed: 29633780]

Rovere M, Powers AE, Patel DS, and Bartels T (2018b). pTSara-NatB, an improved N-terminal acetylation system for recombinant protein expression in E. coli. PLoS ONE 13, e0198715. [PubMed: 29995905]

Rovere M, Powers AE, Jiang H, Pitino JC, Fonseca-Ornelas L, Patel DS, Achille A, Langen R, Varkey J, and Bartels T (2019). E46K-like α-synuclein mutants increase lipid interactions and disrupt membrane selectivity. J. Biol. Chem. 294, 9799–9812. [PubMed: 31048377]

Runwal G, and Edwards RH (2021). The membrane interactions of synuclein: physiology and pathology. Annu. Rev. Pathol. 16, 465–485. [PubMed: 33497259]

Selenko P, Frueh DP, Elsaesser SJ, Haas W, Gygi SP, and Wagner G (2008). In situ observation of protein phosphorylation by high-resolution NMR spectroscopy. Nat. Struct. Mol. Biol. 15, 321–329. [PubMed: 18297086]

Shahmoradian SH, Lewis AJ, Genoud C, Hench J, Moors TE, Navarro PP, Castaño-Díez D, Schweighauser G, Graff-Meyer A, Goldie KN, et al. (2019). Lewy pathology in Parkinson's

disease consists of crowded organelles and lipid membranes. Nat. Neurosci. 22, 1099–1109. [PubMed: 31235907]

Spillantini MG, Schmidt ML, Lee VM-Y, Trojanowski JQ, Jakes R, and Goedert M (1997). α-Synuclein in Lewy bodies. Nature 388, 839–840. [PubMed: 9278044]

Sun J, Wang L, Bao H, Premi S, Das U, Chapman ER, and Roy S (2019). Functional cooperation of α-synuclein and VAMP2 in synaptic vesicle recycling. Proc. Natl. Acad. Sci. USA 116, 11113–11115. [PubMed: 31110017]

Theillet F-X, Binolfi A, Bekei B, Martorana A, Rose HM, Stuiver M, Verzini S, Lorenz D, van Rossum M, Goldfarb D, and Selenko P (2016). Structural disorder of monomeric α-synuclein persists in mammalian cells. Nature 530, 45–50. [PubMed: 26808899]

Vargas KJ, Schrod N, Davis T, Fernandez-Busnadiego R, Taguchi YV, Laugks U, Lucic V, and Chandra SS (2017). Synucleins have multiple effects on presynaptic architecture. Cell Rep. 18, 161–173. [PubMed: 28052246]

Viennet T, Wördehoff MM, Uluca B, Poojari C, Shaykhalishahi H, Will-bold D, Strodel B, Heise H, Buell AK, Hoyer W, and Etzkorn M (2018). Structural insights from lipid-bilayer nanodiscs link α-Synuclein membrane-binding modes to amyloid fibril formation. Commun. Biol. 1, 44. [PubMed: 30271927]

Vranken WF, Boucher W, Stevens TJ, Fogh RH, Pajon A, Llinas M, Ulrich EL, Markley JL, Ionides J, and Laue ED (2005). The CCPN data model for NMR spectroscopy: development of a software pipeline. Proteins 59, 687–696. [PubMed: 15815974]

Wang L, Das U, Scott DA, Tang Y, McLean PJ, and Roy S (2014). α-Synuclein multimers cluster synaptic vesicles and attenuate recycling. Curr. Biol. 24, 2319–2326. [PubMed: 25264250]

Westphal CH, and Chandra SS (2013). Monomeric synucleins generate membrane curvature. J. Biol. Chem. 288, 1829–1840. [PubMed: 23184946]

Whittaker VP (1993). Thirty years of synaptosome research. J. Neurocytol. 22, 735–742. [PubMed: 7903689]

Wiedemann C, Schäfer T, Burger MM, and Sihra TS (1998). An essential role for a small synaptic vesicle-associated phosphatidylinositol 4-kinase in neurotransmitter release. J. Neurosci. 18, 5594–5602. [PubMed: 9671651]

Wilhelm BG, Mandad S, Truckenbrodt S, Kröhnert K, Schäfer C, Rammner B, Koo SJ, Claßen GA, Krauss M, Haucke V, et al. (2014). Composition of isolated synaptic boutons reveals the amounts of vesicle trafficking proteins. Science 344, 1023–1028. [PubMed: 24876496]

Winner B, Jappelli R, Maji SK, Desplats PA, Boyer L, Aigner S, Hetzer C, Loher T, Vilar M, Campioni S, et al. (2011). In vivo demonstration that alpha-synuclein oligomers are toxic. Proc. Natl. Acad. Sci. USA 108, 4194–4199. [PubMed: 21325059]

Xu L, Bhattacharya S, and Thompson D (2019). On the ubiquity of helical α-synuclein tetramers. Phys. Chem. Chem. Phys. 21, 12036–12043. [PubMed: 31135803]

Highlights

- Mutations in αSyn affect the biochemistry, architecture, and function of synapses
- In-cell NMR reveals αSyn's participation in transient interactions at synapses
- αSyn-synapse interactions depend on the integrity of synaptic components
- The 3K mutation in αSyn reduces its ability to participate in synaptic interactions

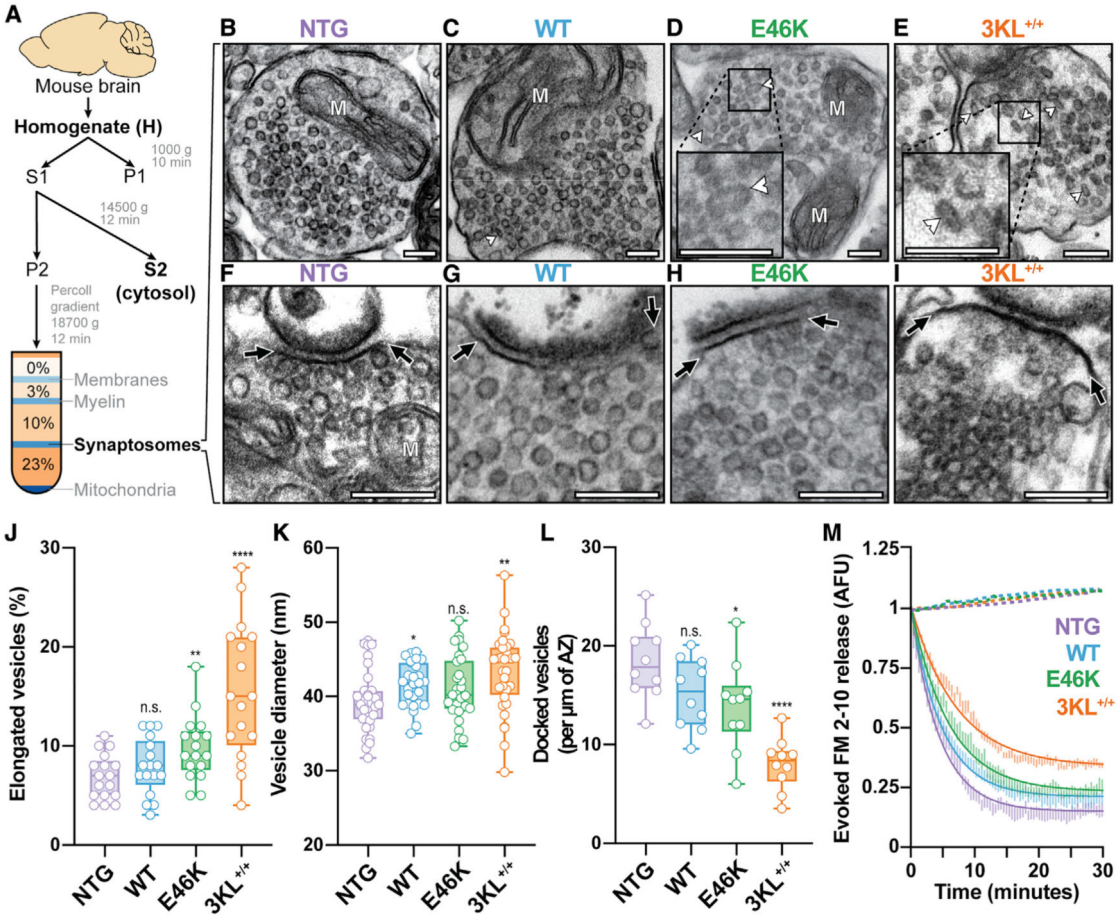

Figure 1. Synaptosomes from 3KL$^{+/+}$ mice show elongated, larger SVs that are not docked to the active zone and have decreased turnover

(A) Diagram of synaptosome purification.

(B–E) Representative transmission electron micrographs of synaptosomes from NTG, hu WT, E46K, and 3KL$^{+/+}$ αSyn transgenic mice, respectively, showing the more abundant elongated SVs (white arrowheads, insets in D and E).

(F–I) Postsynaptic density and active zone (denoted by the darker electronic density and signaled by black arrows) showing SVs docked—within 30 nm of the AZ—to the plasma membrane in synaptosomes of NTG, WT, E46K, and 3KL$^{+/+}$ mice, respectively.

(J) Quantification from (B)–(E) of the percentage of elongated SVs in synaptosomes from at least 4 different mice per genotype. Each dot represents one synaptosome.

(K) The SVs that were not elongated have a larger diameter in 3KL$^{+/+}$ than in E46K, WT, and NTG synaptosomes. Each dot represents a single SV.

(L) Quantification of docked SVs per micrometer of AZ/postsynaptic density (from panels F–I). SVs within 30 nm of the AZ plasma membrane were considered docked. Each dot represents one synaptosome with attached postsynaptic density.

(M) Functional synaptosomes undergo the release of a fluorescent dye upon stimulation. Synaptosome suspensions from NTG, hu WT αSyn, E46K αSyn, and 3KL$^{+/+}$ brains were incubated with FM2–10 dye. In the presence of 1.2 mM Ca^{2+}, fluorescence (Ex/Em, 506/620 nm, normalized to the starting value at t_0) slowly decreased for 30 min after adding

30 mM KCl. Each point is the mean ± SEM of at least 5 different synaptosomal preparations per genotype. A one-phase decay equation was fitted to the data. The dashed lines represent identically prepared synaptosomal fractions from NTG, WT, E46K, and $3KL^{+/+}$ not exposed to Ca^{2+}.

In (J), (K), and (L) quantifications, data are means ± SEM (*p < 0.05, **p < 0.01, ****p < 0.0001 by ANOVA for comparisons of the four genotypes. Student's t test was applied pairwise between $3KL^{+/+}$, E46K, and WT against NTG genotypes; n = 4 different synaptosomal preparations [i.e., 4 mouse brains] per genotype). In (M), we used 6 mice per genotype, except for E46K, where we used 5. We excluded the elongated SVs in quantifying SV diameters. In the electron micrographs, M denotes mitochondria inside synaptosomes. Scale bars: 200 nm.

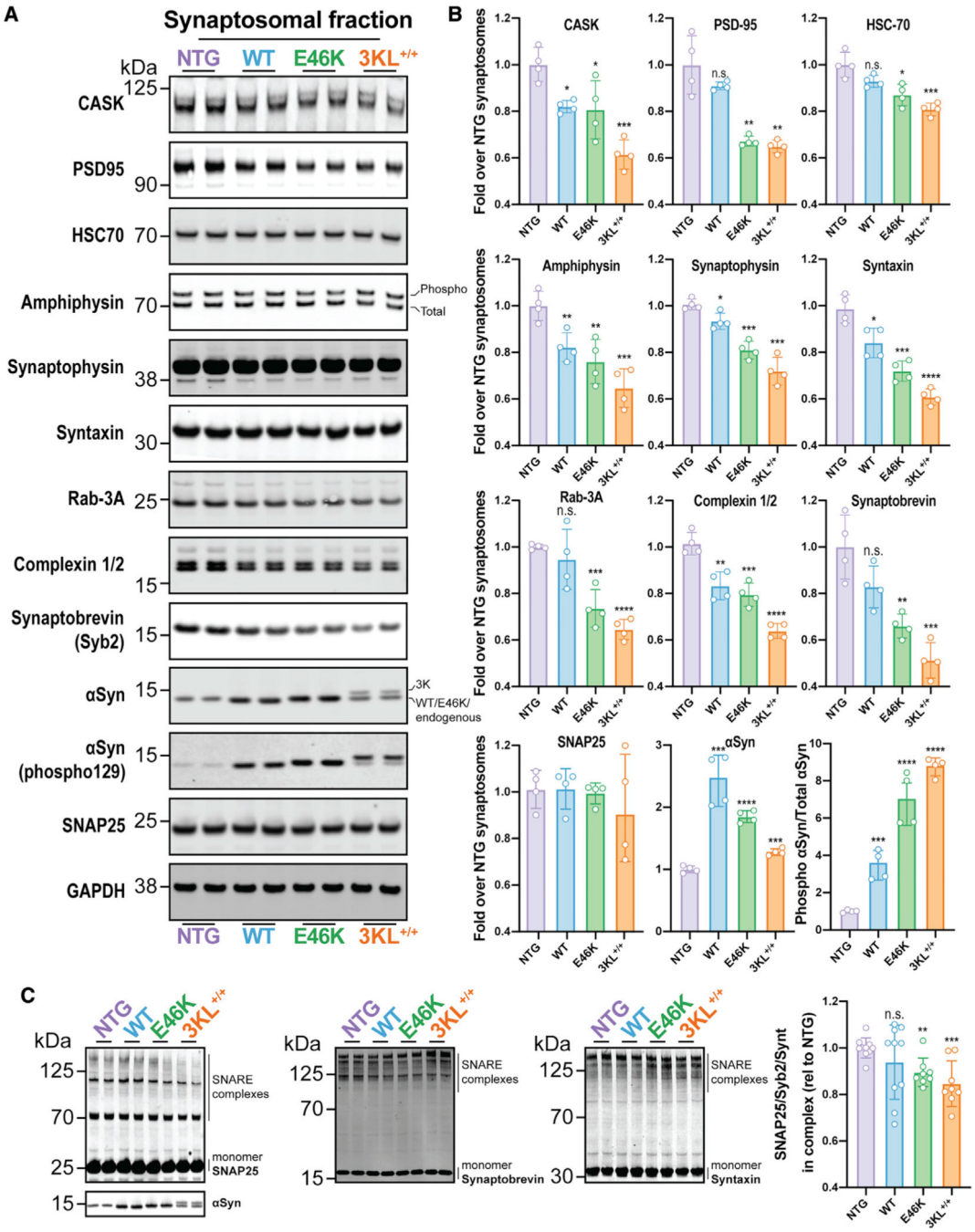

Figure 2. The αSyn multimer-reducing E46K and 3K mutants alter synaptosomal biochemistry

(A and B) Representative western blots of NTG, WT, E46K, and 3KL$^{+/+}$ synaptosomal fractions probed for the denoted proteins (A), and corresponding densitometry quantifications (B) plotted as ratios over the NTG levels.

(C) Immunoblots of non-boiled samples probed for SNAP25, synaptobrevin, and syntaxin higher-order multimers as a proxy for SNARE-complex assembly. The quantification of the ratio between SNAP25, synaptobrevin, and syntaxin in complexes (high-MW bands) and the monomeric signal from the same gel is shown on the right. 10 μg of total protein were

loaded per gel lane, and amounts were normalized to signal of identically prepared samples that underwent boiling to ensure that the concentrations of SNAP25, synaptobrevin, and syntaxin were comparable. Gel lanes represent duplicate experiments. Data are means ± SD. Pairwise comparisons were done by Student's t test, while global comparisons were performed with one-way ANOVA. Criteria for significance relative to NTG were as follows: *$p < 0.05$; **$p < 0.01$; ***$p < 0.001$; and ****$p < 0.0001$. n = 4 different synaptosomal preparations (i.e., mice) per genotype. Each dot in the bars represents a single mouse brain preparation).

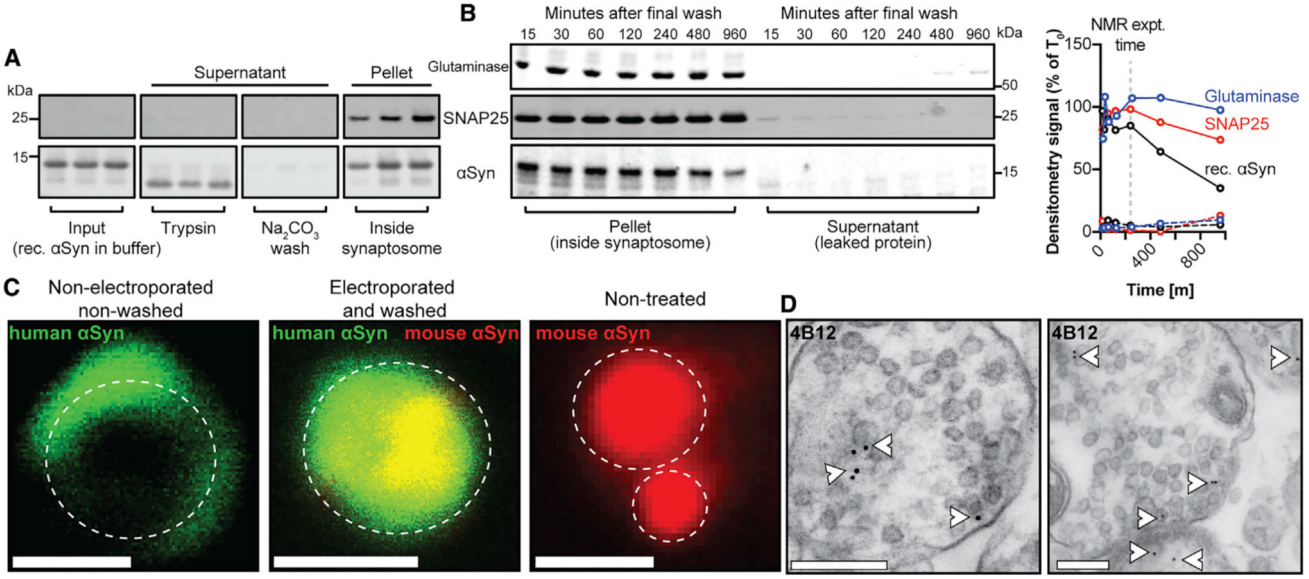

Figure 3. Exogenous αSyn is delivered into and remains inside synaptosomes

(A) Semiquantitative western blot of intra-synaptosomal αSyn after electroporation and subsequent washes and trypsin treatment. Data are shown for 3 biological replicates. Note the short products of αSyn cleavage in the trypsin digestion lanes.

(B) Time course of recombinant αSyn and endogenous glutaminase and SNAP25 retention after electroporation. Less than 15% of αSyn, glutaminase, and SNAP25 signal is lost from the synaptosomes during the first 4 h of incubation post-electroporation, the time interval employed in our NMR experiments. In the quantification plot, solid lines represent the signal in the pellet measured at the given times after electroporation, while the dashed lines depict signal intensities from the corresponding supernatants, reflecting protein leakage.

(C) Immunofluorescent microscopy of αSyn inside synaptosomes from 12-month-old NTG mice. 4B12 (green channel) recognizes only the human (recombinant) αSyn, while C20 (red channel) recognizes both mouse and human αSyn. The panel to the far left shows synaptosomes in the presence of recombinant αSyn without electroporation and washing steps (i.e., αSyn accumulates on the synaptosomal outer membrane). The adjacent panel shows electroporated synaptosomes, where recombinant αSyn adopts the same uniform localization as endogenous murine αSyn (immunofluorescence shows complete colocalization, in yellow). Untreated synaptosomes (on the right) were not exposed to recombinant αSyn or electroporation and showed a uniform distribution of endogenous αSyn. Scale bar: 1 μm. White dashed lines in confocal images represent the contour of individual synaptosomes.

(D) 4B12 was used for immunogold labeling of recombinant αSyn in electron micrographs (two different samples; white arrowheads) to confirm synaptosomal membrane preservation and localization of recombinant αSyn inside the intact synaptosome. Scale bar: 200 nm. Gold particles are 15 nm in diameter.

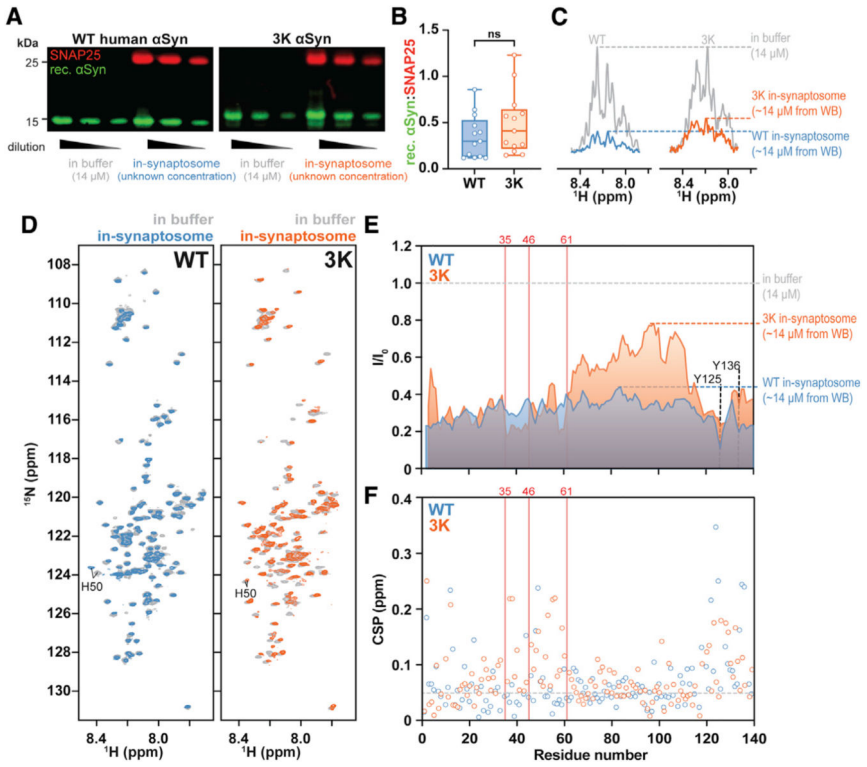

Figure 4. NMR spectra of WT and 3K ^{15}N-human αSyn electroporated into mouse brain synaptosomes

(A) Semiquantitative western blotting of known reference amounts of recombinant αSyn compared to electroporated synaptosomes shows that both WT and 3K αSyn are delivered into synaptosomes with similar efficiency.

(B) Ratio of the densitometries of recombinant αSyn versus the endogenous synaptosomal marker SNAP25. Because both WT and 3K αSyn are electroporated with similar efficiencies, differences in their αSyn:SNAP25 ratio are not significant.

(C) 1D ^{1}H-^{15}N-filtered NMR spectrum of WT (left) and 3K (right) αSyn in NMR buffer (gray spectra) and inside synaptosomes purified from NTG mouse brains (blue and orange spectra, respectively).

(D) 2D ^{1}H-^{15}N HSQC NMR spectra of WT (left) and 3K (right) αSyn in NMR buffer (gray spectra) and inside synaptosomes purified from NTG mouse brains (blue and orange spectra, respectively). Intrasynaptosomal locus of the electroporated αSyn was validated in Figure 3. Both WT and 3K recombinant hu αSyn had been expressed as N-terminally acetylated proteins.

(E) Quantification of NMR signal intensity ratios between in-synaptosome (I) and in-buffer (I_0) signals for both WT (blue) and 3K (orange) αSyn. The three E→K substitutions in 3K αSyn are numbered in red and marked by red lines. The dashed gray line represents the expected NMR signal intensity of αSyn at a 14 μM concentration *in vitro*.

(F) Residue-resolved combined CSP of backbone amide resonances between αSyn in buffer and inside synaptosomes for both WT (blue) and 3K (orange) αSyn. The dashed gray line marks a significance level of one standard deviation (SD) from the chemical shift perturbation mean.

In (B), Student’s t test revealed no significant difference between the ratios of SNAP25:recombinant αSyn in the two variants.

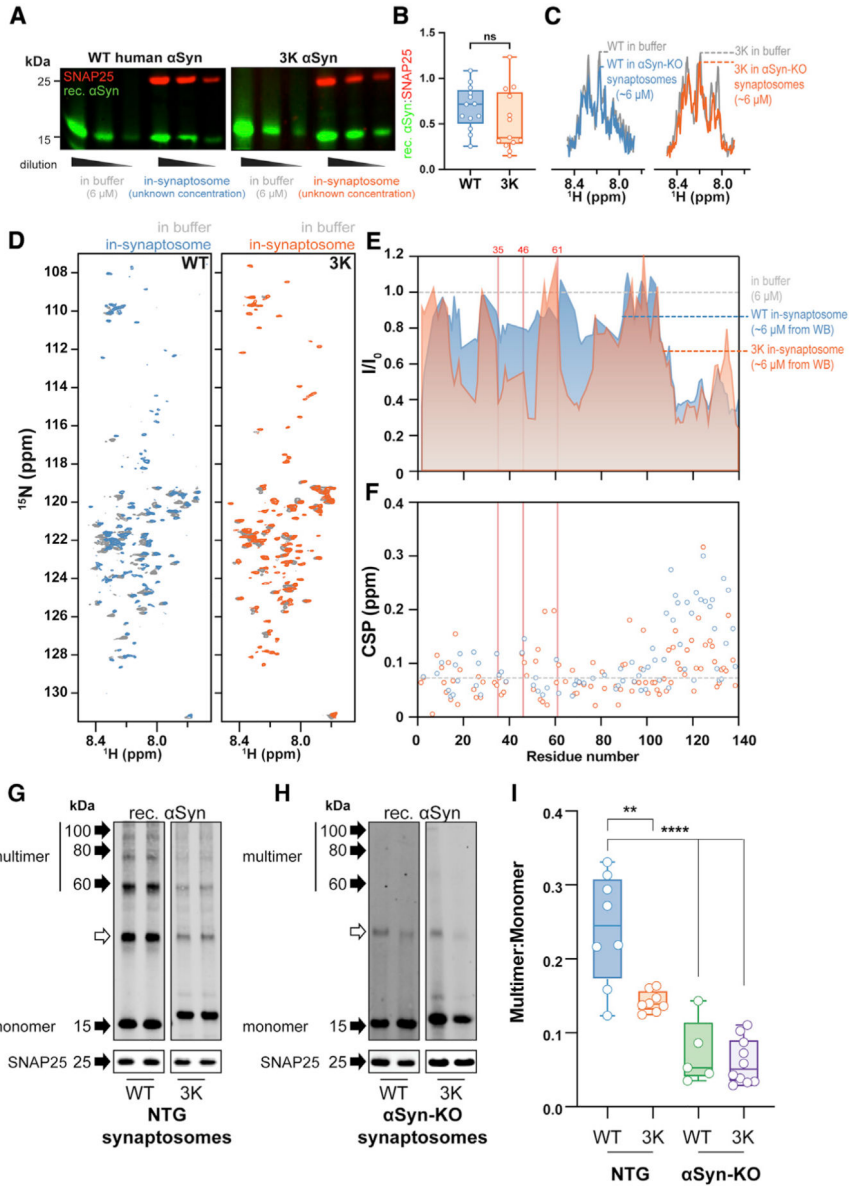

Figure 5. In the absence of endogenous αSyn, recombinant αSyn fails to multimerize

(A) Semiquantitative western blotting of a known reference of recombinant WT and 3K hu αSyn (6 μM) and the electroporated synaptosomal sample. The densitometry comparison shows that the recombinant αSyn inside synaptosomes reached a concentration of ~5.5 and 6.5 μM for WT and 3K αSyn, respectively.

(B) The ratio of endogenous SNAP25 (red signal in WB) to recombinant αSyn (green signal in WB) is the same in both WT and 3K experiments.

(C) 1D ^{1}H-^{15}N-filtered spectrum of WT and 3K αSyn in αSyn-KO synaptosomes (i.e., without endogenous αSyn).

(D) 2D ^{1}H-^{15}N HSQC NMR spectra of WT and 3K αSyn in NMR buffer (gray spectra) and inside synaptosomes purified from αSyn-KO mouse brains (blue and orange spectra, respectively). WT and 3K αSyn are N-terminally acetylated.

(E) Quantification of NMR signal attenuation between “in-synaptosome” (I) and “in-buffer” (I_0) signals for WT and 3K αSyn. The dashed gray line represents the expected signal for a sample made entirely of monomeric, unfolded αSyn.
(F) Residue-resolved combined chemical shift perturbations (CSPs) of backbone amide resonances between αSyn “in-buffer” and “in-synaptosome” for WT and 3K αSyn (blue and orange dots, respectively). The dashed gray line marks a significance level of one standard deviation (SD) from the mean.
(G) Inside synaptosomes, electroporated recombinant WT αSyn forms multimers that resemble those found in intact cells, while the 3K mutation significantly reduces their formation.
(H) In the absence of endogenous αSyn, both WT and 3K recombinant αSyn fail to multimerize inside synaptosomes.
(I) Quantification of the multimer-to-monomer ratio of WT and 3K αSyn inside synaptosomes with and without endogenous αSyn.
In (B), a Student’s t test revealed no significant difference between the ratios of SNAP25:recombinant αSyn in the two variants. **$p < 0.01$, ****$p < 0.0001$ by one-way ANOVA (global) and Student’s t test (pairwise) that was applied between 3K and WT in both NTG and αSyn-KO synaptosomes; $n \geq 5$ different experiments per condition.

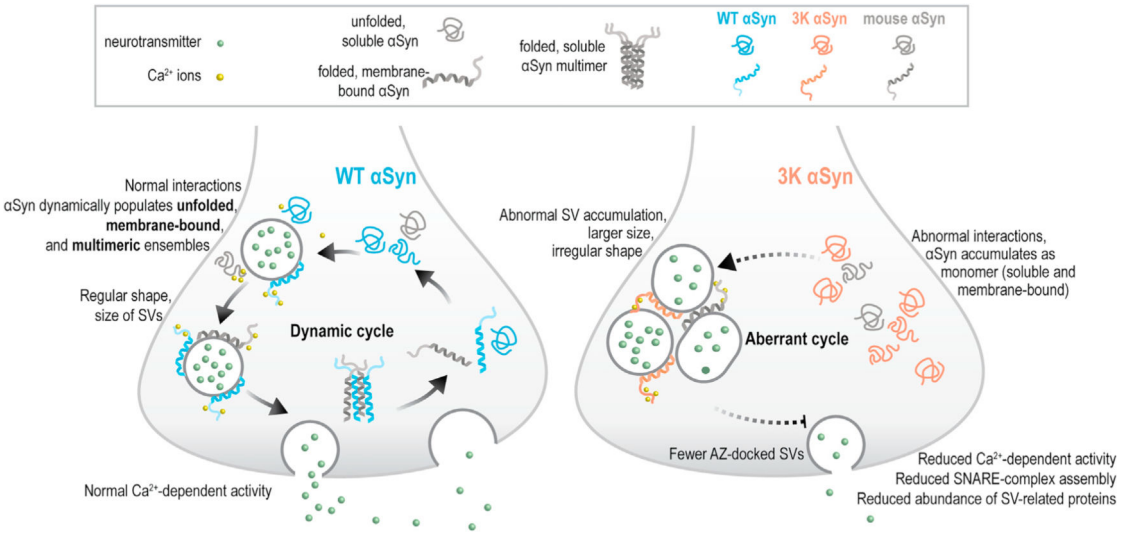

Figure 6. Putative model of αSyn dynamics and effects at the synapse under normal and pathological scenarios based on findings herein

Under physiological conditions, WT αSyn helps mediate the assembly of the SNARE complex by bringing together SVs in the proximity of the active zone in a Ca^{2+}-dependent manner. Our spectroscopic data suggest that αSyn may do this in a dynamic fashion as (NMR-visible, blue and orange) unfolded monomers bind to synaptic components—including multimerization events templated by NMR-invisible endogenous mouse αSyn (in gray)—through their N-terminal region and to other proteins as well as Ca^{2+} through their negatively charged C-terminal region. These interactions promote αSyn conformational rearrangement, attenuating its NMR signal. The emerging conformers facilitate SV docking to the presynaptic plasma membrane and SNARE-complex assembly. Multimeric αSyn then disassembles into monomers that are ready to reenter the cycle. Multimer-deficient 3K αSyn (and perhaps excess WT αSyn in pathologic scenarios) remains more prominently in a monomeric and membrane-bound state that cannot promote proper SV docking and SNARE-complex assembly, and thus synaptic activity. The abnormal accumulation of SVs away from the active zone may promote their increase in size and irregular shape.

KEY RESOURCES TABLE

REAGENT or RESOURCE	SOURCE	IDENTIFIER
Antibodies		
CASK	ABCAM	Cat# ab3383; RRID: AB_303761
PSD95	ABCAM	Cat# ab238135
HSC70	SANTA CRUZ	Cat# sc-7298; RRID: AB_627761
Amphiphysin II	SANTA CRUZ	Cat# sc-13575; RRID: AB_626753
Synaptophysin	THERMO FISHER SCIENTIFIC	Cat# PA1–1043; RRID: AB_2199026
Syntaxin	ABCAM	Cat# ab188583
RAB-3A	THERMO FISHER SCIENTIFIC	Cat# PA1–770; RRID: AB_2177381
Complexin 1/2	Synaptic systems	Cat# 122 003; RRID: AB_2619793
Synaptobrevin	Synaptic systems	Cat# 104 2011
4B12	THERMO FISHER SCIENTIFIC	Cat# MA1–90346; RRID: AB_1954821
pSer129	ABCAM	Cat# ab51253; RRID: AB_869973
SNAP25	ABCAM	Cat# ab5666; RRID: AB_305033
GAPDH	ABCAM	Cat# NC0758042
EEA1	BD Biosciences	Cat# BDB610457
Bacterial and virus strains		
BL21	New England Biolabs	Cat# C2527H
Chemicals, peptides, and recombinant proteins		
^{15}N ammonium chloride	Cambridge Isotope Laboratories	Cat# NLM-478-PK
D-Glucose (U-$^{13}C6$, 99%)	Cambridge Isotope Laboratories	Cat# CLM-1396–5
D_2O	Sigma-Aldrich	Cat# 151882–100G
Percoll	Sigma-Aldrich	Cat# P4937–500ML
Experimental models: Organisms/strains		
Mouse: C57BL6;Tg(SNCA*E35K-E46K-E61K)3KL-3798	The Jackson Laboratory	JAX# 032799
Mouse: B6N.Cg-Tg(SNCA*E46K)3Elan/J	The Jackson Laboratory	JAX# 018768
Mouse: C57BL6;Tg(SNCA*WT)WT-3877	Nuber et al., 2018	N/A
Mouse: C57BL/6NCrl	Charles River	CAT# C57BL/6NCrl
Mouse: C57BL/6NTac SNCA KO	The Jackson Laboratory	JAX# 016123
Software and algorithms		
GraphPad Prism	GRAPHPAD	https://www.graphpad.com/
TOPSPIN 3	Bruker/ Biospin	N/A
ccpNMR	CCPN	https://www.ccpn.ac.uk/